Stony Brook University

Synthesis, structure, and electrochemical Li-ion intercalation properties of $Li_zTi_5O_{12}$ - $Li_2Ti_3O_7$ nanocomposites

A Thesis Presented

by

Zelun Sun

to

The Graduate School

in Partial Fulfillment of the

Requirements

for the Degree of

Master of Science

in

Materials Science and Engineering

Stony Brook University

May 2014

Stony Brook University

The Graduate School

Zelun Sun

We, the thesis committee for the above candidate for the

Master of Science degree, hereby recommend

acceptance of this thesis.

Dong Su – Thesis Advisor

Scientist, Center for Functional Nanomaterials, Brookhaven National Laboratory

Dilip Gersappe – Second Reader

Professor, Materials Science and Engineering

T. A. Venkatesh – Third Reader

Associate Professor, Materials Science and Engineering

This thesis is accepted by the Graduate School

Charles Taber

Dean of the Graduate School

Abstract of the Thesis

Synthesis, structure, and electrochemical Li-ion intercalation properties of Li4Ti5O12-Li2Ti3O7 nanocomposites

By

Zelun Sun

Master of Science

in

Materials Science and Engineering

Stony Brook University

2014

Lithium ion batteries (LIBs) are expected to be used for energy storage in electric vehicles (EVs) as well as for load leveling for photovoltaic power generation or wind power generation. For the LIBs in EVs, Spinel-type $Li_4Ti_5O_{12}$ (LTO) has been investigated as an alternative anode material. However, the disadvantage of LTO as an anode is the low electronic conductivity resulting from its insulating ionic crystal structure. On the other hand, ramsdellite-type $Li_2Ti_3O_7$ (RLTO) already has good electrical conductivity.

In our research, LTO nano powders were synthesized/reprocessed by RTP processing and the stability of $Li_4Ti_5O_{12}$ was successfully studied by XRD measurement and half-quantitate calculation based on XRD results. By introducing a new method to synthesis/process $Li_4Ti_5O_{12}$, we were able to synthesis a new $Li_4Ti_5O_{12}$ - $Li_2Ti_3O_7$ nanocomposite.

The components were also studied by changing the annealing environment (annealing temperature, holding time, and atmosphere). This shows a final state of LTO using rapid thermo annealing as a synthesis/reprocessing method can be reached when annealing temperature is higher than 900 ℃ or the holding time ≥ 60 seconds at 880 ℃, with a result of a composition of 25.4% $Li_2Ti_3O_7$ and 74.6% $Li_4Ti_5O_{12}$.

The electrochemical properties of annealed LTO were also studied which showed a better capacity and better cyclability.

Key words: $Li_4Ti_5O_{12}$; $Li_2Ti_3O_7$; lithium ion battery; anode

Contents

List of Figures

List of abbreviations

LIB……Lithium-ion battery

EV……Electric vehicle

HEV……Hybrid Electric vehicle

RTP……Rapid thermo processing

XRD……X-ray diffraction

TEM……Transmission electron microscopy

STEM……Scanning transmission electron microscopy

SAED……Selected area electron diffraction

HR-TEM……High resolution transmission electron microscopy

LTO……$Li_4Ti_5O_{12}$

RLTO……$Li_2Ti_3O_7$

Acknowledgement

I would like to first express my sincere gratitude to my thesis advisor, Dr. Dong Su for his generous support, patience, immense knowledge and mentoring through my research and master thesis. I have enjoyed learning from him.

Beside my advisor, I would like to thank the rest of my thesis committee: Prof. T. A. Venkatesh and Prof. Dilip Gersappe for their suggestions on my thesis.

This research was conducted at Center for Functional Nanomaterials and Chemistry Department in Brookhaven National Laboratory supported by the U.S Department of Energy. I would like to thank whole electron microscopy group and electronic nanomaterials group for providing materials characterization and materials synthesis facilities, especially Dr. Dmytro Nykypanchuk for his training on XRD, Dr. Mingzhao Liu for his training on rapid thermo process machine, Dr. Xiqian Yu on cell assembling and characterizing and Dr. Kai He, Dr. Lihua Zhang, Dr. Chang-Yong Nam, Dr. Yugang Zhang for their guidance on XRD and TEM.

I am also thankful to Xianghai Meng, Tianyi Zhou and Gordon Chin for their advice on my research and career.

Last but not least, I take this opportunity to express deepest gratitude to my beloved parents and grandparents for their continuous support throughout my life.

Chapter 1 Introduction

1. Rechargeable Li-ion Battery

The growth of population is matched by a heavy demand of energy. Also, as we entered the second decade of the twenty-first century, we have reached a challenge of global warming and the finite of fossil fuels. Based on the speed of population and economics growth, world energy consumption in 2100 will be three times as much as in 2010. The energy consumption at present are mostly from burning the nonrenewable fossil fuels.

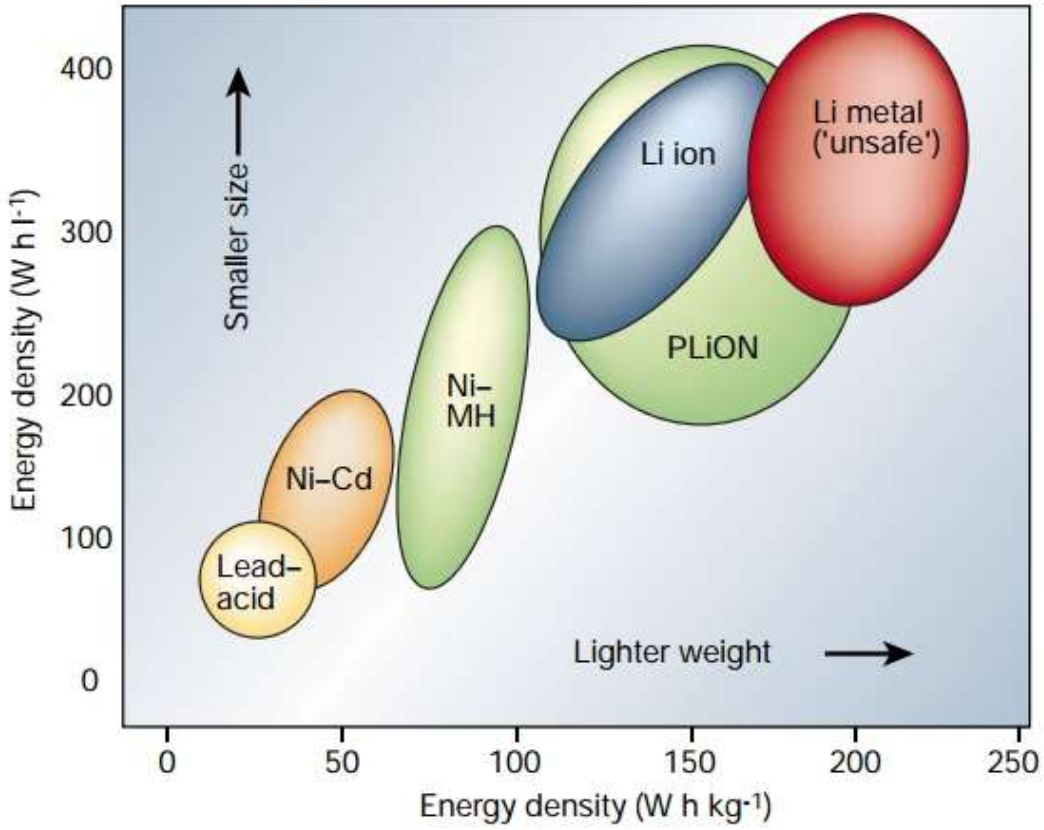

Figure 1.1 Comparison of the different battery technologies in terms of volumetric and gravimetric energy density (Adapted from J.-M. Tarascon, M. Armand, Nature, 414 (2001) 359)

Therefore, the use of new and renewable sources of energy to replace conventional energy more show pressing. Particularly, solar radiation, wind, waves and geothermal energy will demand the demand of efficient energy storage system since these sources are restricted in location.

Among different energy storage technique, rechargeable Li-ion battery (LIB) technology has the highest energy density (as shown in figure 1.1). The Li-based technology can achieve the volumetric energy density up to 400 Wh/L, and the gravimetric energy density up to 200 Wh/kg. Currently, LIB is generally used for portable devices, e.g. computers, communication devices, large scale system in electric cars, required by today's mobile world. It's facilitating the development of storage system for more applications with high energy density.

1.1. History of developments in Li-ion battery

The beginning of research on lithium batteries goes back to the 1960s. The first primary cell (non-rechargeable) was assembled in 1970s which shows the advantage of Li metal using as electrode.[1] Li is the most electropositive (-3.04 V versus standard hydrogen electrode) as well as the lightest (equivalent weight M= 6.94 g/mol) metal among all the elements. The energy density of Li metal is up to 3860 Ah/kg theoretically while the energy density of Zn and Pb metal is only 820 Ah/kg and 260 Ah/kg, respectively. Owing to the variable discharge rate and high capacity, the applications can be found in power sources like watches, calculators or other portable devices. At the same time, reversible reactions between many inorganic compounds and alkali metals were found. This discovery were later identified as intercalation, was crucial in the development of high energy density rechargeable Li systems. In 1972, the concept of electrochemical intercalation and its potential use were clearly defined.[2, 3]

In 1972, Exxon[4, 5] utilized TiS_2 s the cathode, Li metal as the anode and Lithium perchlorate in dioxolane as the electrolyte. Being as a very beneficial layered-type structure, TiS_2 was the best intercalation compound available at that time. But the system was not viable because it soon encounter a dendritic growth of Li-metal anode during each discharge-charge cycle. This kind of battery wasn't commercialized because the dendritic growth would cause safety issues.

In 1980, Armand[6] demonstrated the so-called Li-ion or rocking–chair technology which solved the dendrite problem, inherently made the Li batteries much safer. This technology replaced Li-metal anode with some intercalation materials. Over the same period, Goodenough successfully synthetized layered intercalation materials $LiMO_2$ (M= Co, Ni, Mn) and demonstrated their reversible process of lithiation and delithiation.[7, 8]

In 1989 Sony Corporation patented a $C/LiCoO_2$ rocking- chair cell and then commercialized it by 1990, named the cell Li-ion battery.[9]

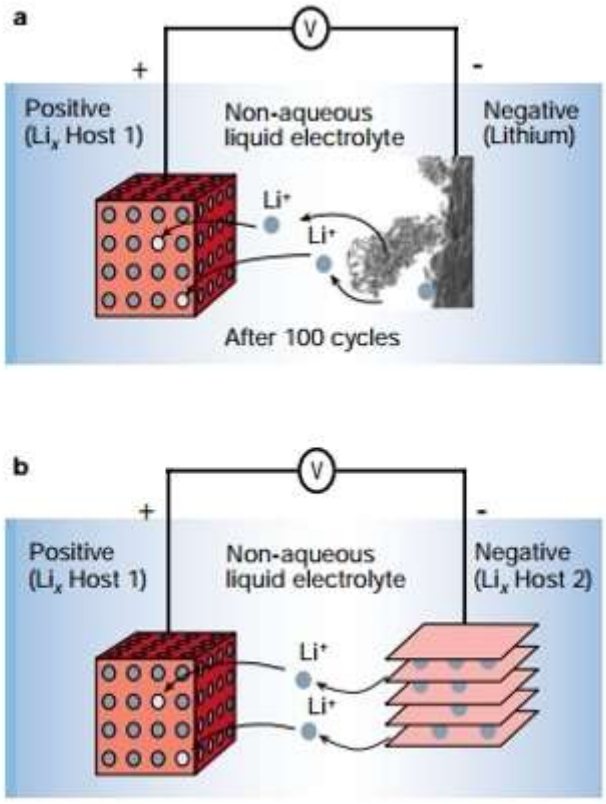

Figure 1.2 Schematic representation and operating principles of Li batteries (Adapted from J.-M. Tarascon, M. Armand, Nature, 414 (2001) 359)
a, Rechargeable Li-metal battery b, Rechargeable Li-ion battery.

1.2. Working principle

Figure 1.2 and 1.3 schematic shows working principle of an intercalation Li-ion battery.[10] A Li-ion battery contains cathode, anode and electrolyte. During the discharge process, the electrons of anode migrate to the cathode through the external circuit, while lithium ions go through the electrolyte then form the cathode. Reversing this process results in the charge process, a current flow from anode to cathode and lithium ions migrate to the anode. This working model requires Li ions can be stored in both anode and cathode materials.

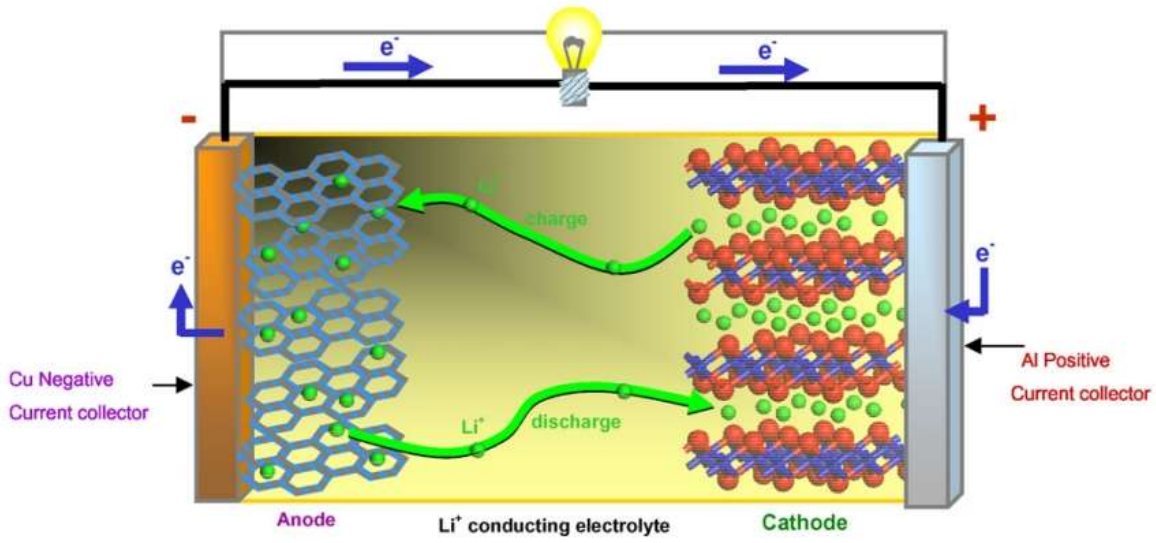

Figure 1.3 Schematic illustration of the discharging and charging process of a lithium rechargeable battery (Cited from http://www.intechopen.com/books/energy-storage-technologies-and-applications/electrochemical_energy_storage)

The working mechanisms of LIB fall broadly into: [11]

1) Intercalation reaction mechanism, e.g.,

$$(1\text{-}x)Li + LixCoO_2 \leftrightarrow LiCoO_2$$

This is the most common reaction of all and people use $LiCoO_2$ developed the rocking-chair battery. Also, the first commercialized $LiCoO_2$/C is due to this reaction mechanism. Normally, we are using layered-structure material (space group R-3m), e.g. $LiMO_2$ (M=Co, Ni, Mn, etc.). During its charging-discharging process, the charging-discharging curve shows the behavior of solid solution, as an oblique line. This can be explained by lattice gas model. The capacity of battery is determined by gain or loss of electrons and accommodation of Li ions.

2) Conversion reaction mechanism, e.g.,

$$2Li + MnO \leftrightarrow Li_2O + Mn$$

This reaction mechanism was proposed by Poizot Et al in 2000 at NATURE.[12]The reaction can be achieved in metal fluoride, metal sulfide, metal phosphide and metal hydride. Irreversible capacity loss is pretty obvious because of the polarization during the reaction.

3) Phase transition mechanism, e.g.,

$$xLi + xFePO_4 \leftrightarrow XLiFePO_4$$

The first phase can slowly or immediately transfer into a second phase during the charging-discharging process. According to Nernst equation, the charging-discharging curve shows a platform.

4) Reversible chemical bonding mechanism, e.g.,

$$4Li + Li_2C_6O_6 \leftrightarrow Li_6C_6O_6$$

This reaction mechanism was first proposed by LRCS[13] by using hydroxyl organic matter as a lithium-stored material. It has a poor performance on both theoretically volumetric energy density and conductivity. But people believe it shows the potential of sustainable energy because the material can be found in all living organisms.

5) Surface charging mechanism.

The mechanism is often used in super capacitor. When electric field is applied, anions and cations in liquid electrolyte will be gathered at the surface of electrode materials. The charging-discharging curve shows a platform. Cell capacity depends on the electric constant, i.e. specific surface area, thickness of the electrode materials. Also, the species of ion in electrolyte will dominate the performance of cell.

6) Organic free radical mechanism

Organic free radical can be taken advantages of absorbing unpaired electrons, utilizing polymerization reaction or oxidation reaction to form closed shell molecules. This mechanism shows good reaction safety and a promising sustain. The disadvantage is, as mentioned above in

reversible chemical bonding mechanism, the poor performance on theoretically volumetric energy density.

7) Under potential deposition mechanism

There was reported that, at 0.0 V vs. Li+/Li, lithium storage can be happened in cellular and mesoporous material. [14]

8) Interfacial charging mechanism

When Maier's group was searching on the conversion reaction of LiX/M (where M means transition metals), at 0-1.2 V vs. Li+/Li, there was a capacity showed. According to the thermodynamic calculation, the chemical potential of this reaction should be higher than 1.2 V, also, there's no way of LiX and M to storage Li ions. Thus, the conception of interfacial charging mechanism has been proposed.

Compared to other kinds of secondary chemical energy, Li-ion battery has shown advantages such as:

(1) High working potential. Up to 3.6 V per cell.
(2) High energy density.
(3) A broad range of working temperature
(4) High energy efficiency.
(5) Long cycling life.
(6) High charging-discharging rate performance.
(7) Low self-discharge.
(8) No memory effect.
(9) Green non-polluting.

2. Why it is so hard to improve the energy density of lithium battery

2.1. Introduction

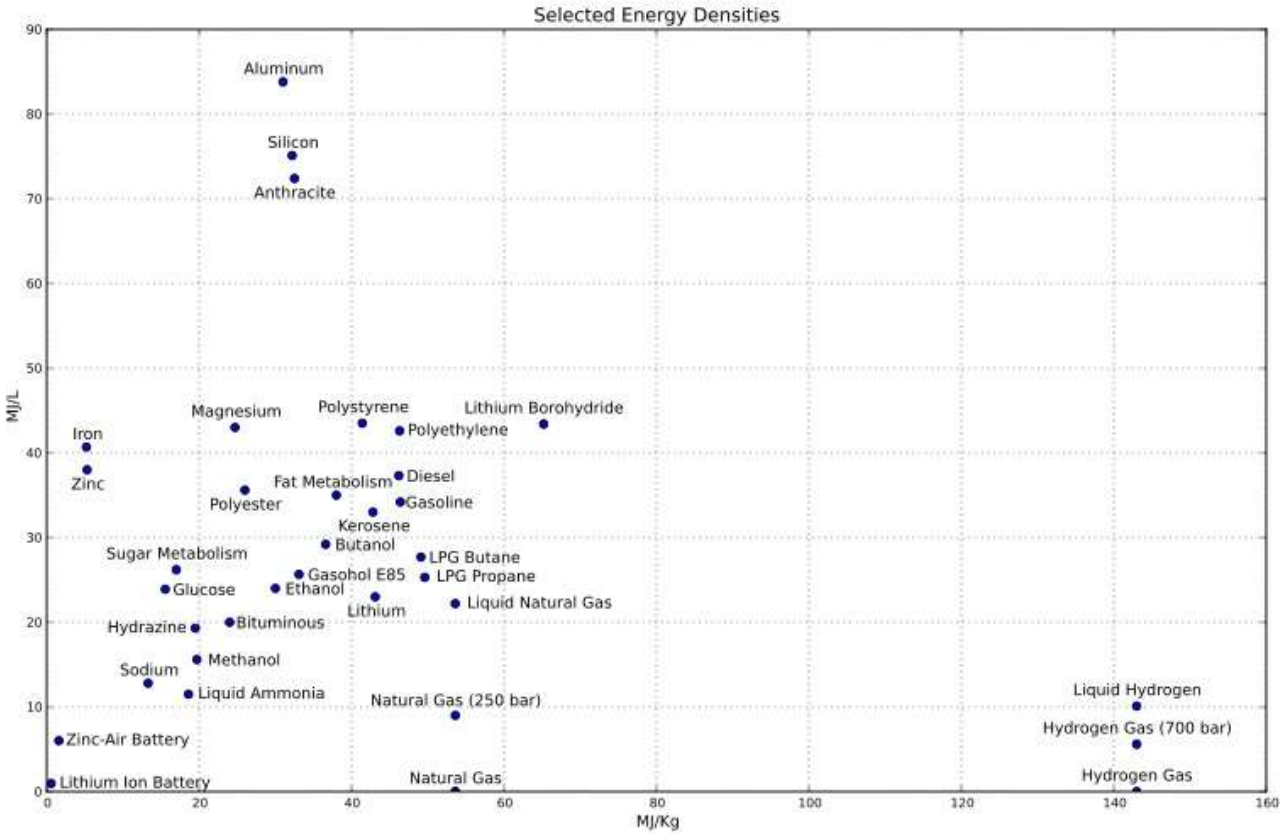

Figure 1.4 Selected energy densities plot (Cited from http://en.wikipedia.org/wiki/File:Energy_density.svg)

As shown above, it's a plot of selected energy densities from Wiki. The point of Lithium ion battery only shows in the corner at the left bottom which means Lithium ion battery holds a relative low energy density and need to be improved urgently. If we find the points of gasoline, diesel, ethane and natural gas in this plot, there always shows better energy densities.

Gasoline has an energy density of 46.4 MJ/Kg while lithium has an energy density of 43.1 MJ/Kg. It seems possible to have a lithium battery with a competitive energy density. But a primary lithium battery holds an energy density of 1.8 MJ/Kg and 0.35-0.875 MJ/Kg can only be reached in a secondary lithium battery. What really restrict the energy density of LIB and why it is so hard to improve the energy density of LIB?

2.2. Redox reaction

The mechanisms of energy carriers like fuels and batteries are all based on chemical reaction especially redox reaction.

As we mentioned at the mechanism of battery above, the essence of a battery is the transfer of electrons from anode to cathode through the circuit.

Since electron is the source of energy, we can calculate the density of electron to evaluate the energy density. Here we assume works are always the same when we have one electron transferred (It is obviously wrong, the work is also determined by different type of oxidation and reduction, but if we consider about the common batteries and fuels, the assumption is right).

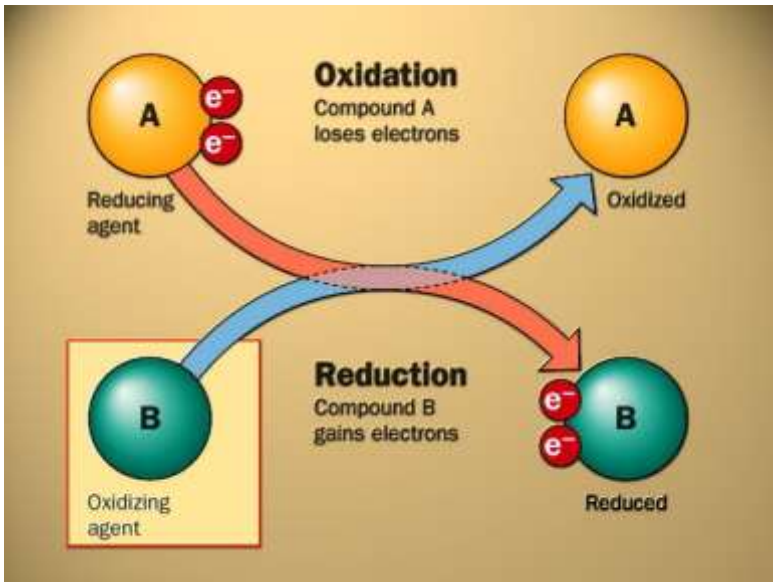

Figure 1.5 Mechanism of redox reaction (Cited from http://student-sc.blogspot.com/2012/12/chemistry-form-5-chapter-3-redox.html)

The electron density of energy carriers depends on electron transfer rate if we only calculate the electron density by mass (if we calculate the electron density by volume, an answer like solid>liquid>gas is easy to get and understand). Inner electrons of atoms are barely active to reactions, works are done by the transfer of outer electrons. The electron transfer rate is the number of reaction electrons divided by the number of total electrons.

E.g.

1) H_2-2e^- =2H^+

Since one H_2 molecule has two electrons and they are all transferred, the electron transfer rate is 100%

2) Li-e^- =Li+

There are 3 electrons in a lithium atom, only one is transferred, the electron transfer rate is 33.3%.

3) Zn-2e^- =Zn^{2+}

The electron transfer rate is 2/30=6.7%.

It is easy to find that the best two elements to choose as an energy carrier is C and H which are the components of gasoline, natural gas and other fuels we are using today. It is an optimization already as we use gasoline or diesel to drive a car. Using lithium battery as an energy source has "inherent problems"

2.3 Electrolyte

There are 4 main functional parts in a lithium battery, they are cathode, anode electrolyte and separator.

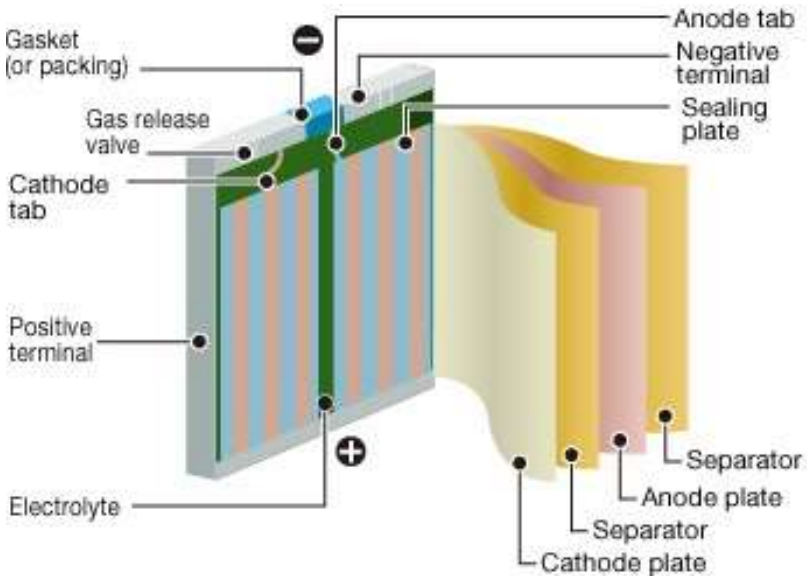

Figure 1.6 A schematic show of the components in lithium ion battery (Cited from http://www.megagraphite.com/products/byapplication/batterygrade)

The ideal function of electrolyte is transferring lithium ions. So electrolyte should have a good conductivity of lithium ions and must not be a conductor of electrons. It also means, there will be no current if we don't add a voltage or have a circuit. As long as there's an external circuit, the electron can move from anode to cathode through it.

As a result, the energy density is even lowered after adding electrolyte which is not doing any work. For a well-known 18650 cell with 42g unit weight, it contains only 0.65g lithium metal, approximately 1.5% of the total mass. Normally, electrolyte account for 15% of the total mass.

2.4. Electrode materials.

As the figure 1.3 showed above, it's a schematic illustration of the discharging and charging process of a lithium rechargeable battery, the structures of both electrodes are ordered. The reason of using ordered structures is to produce a current, also, the redox reaction has to be done at the electrodes.

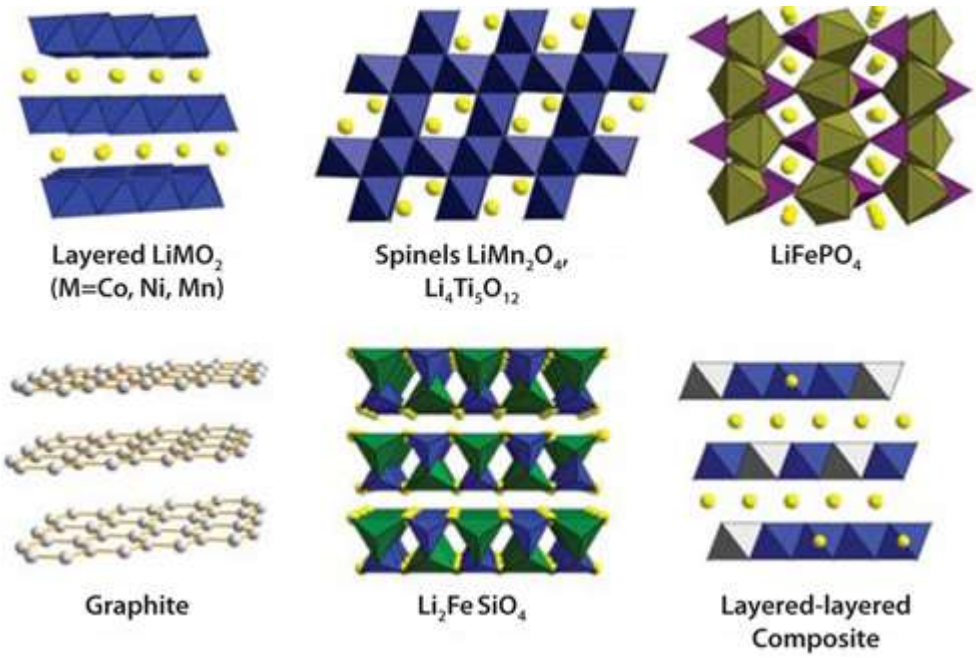

Figure 1.7 Structures of electrodes using in lithium batteries (Cited from http://www.sigmaaldrich.com/technical-documents/articles/material-matters/electrode-materials-for-lithium-ion-batteries.html)

To make the lithium transfer efficient in the anode side during the charging process, there's a solidified structure (graphite) using as the anode to organize the lithium also lower the entropy. This kind of battery design reduce the energy density.

At cathode side, the same problem also occur. People also use a solidified structure on the cathode to achieve the goals with more problems coming out.

In a layered $LiMO_2$ (M=Co, Ni, Mn), MO_2 can form several layers on cathode base. During the charging process, the electrons are gathered at cathode and lithium ions intercalate into MO_2 cathode to form $LiMO_2$ layered structure. However, the number of lithium ion on cathode material is limited because once there's too few lithium ions on the cathode, the structure will collapse without an ability to recover itself (figure 1.9). There must be an amount of lithium ion at the cathode, normally 50%, to maintain the integrity of such a layered structure.

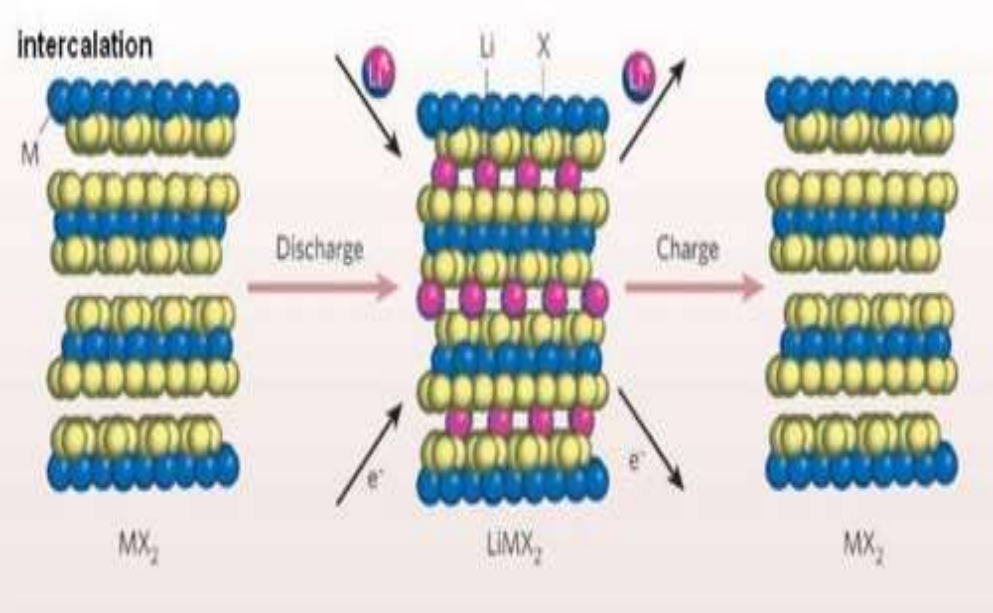

Figure 1.8 Intercalation of lithium ions (Cited from http://tymkrs.tumblr.com/post/7846476684/lithium-ion-battery-how-does-it-work)

Figure 1.9 Collapse of layered structure happens in macro world (Cited from http://www.101toys.com.tw/chuansheng/front/bin/ptdetail.phtml?Part=126019)

2.5. Conclusion

There are quite a lot limits on design of rechargeable lithium battery. Lithium intercalations, controlled the distribution at electrode surface of lithium ions, using electrolyte and the specified structures of electrodes, these are all at the cost of the loss of energy density.

The structure of electrodes is the main problem of lithium battery. People have used all possible elements on oxidation and reduction. Some use nano materials. Nano materials have larger specific surface areas and better electrochemical properties. But it's hard to reach a high energy density of nano material, the nano size makes it hard to be packed. Also, the separator in a battery is micron level so that nano materials can go through the separator and short the circuit.

Along with the research on lithium ion battery, we believe, utilizing nano materials can reach a high energy density of commercial lithium ion battery.

3. $Li_4Ti_5O_{12}$ as an anode material for Li-ion batteries

3.1. Introduction

The first commercial cell was introduced in the 1980s by Matsushita. It's a Wood's metal (a low-melting alloy containing Bi, Pb, Sn and Cd). Nowadays, we are only using two kinds of commercialized anode materials: carbon based (primarily graphite) and $Li4Ti_5O_{12}$ (LTO) materials.

By utilizing different kinds of chemical or physical modifications, carbon display a more and more promising electrochemical performance. Reversible capacities around 450 m Ah/g for graphite (372 m Ah/g for the end compound LiC_6).

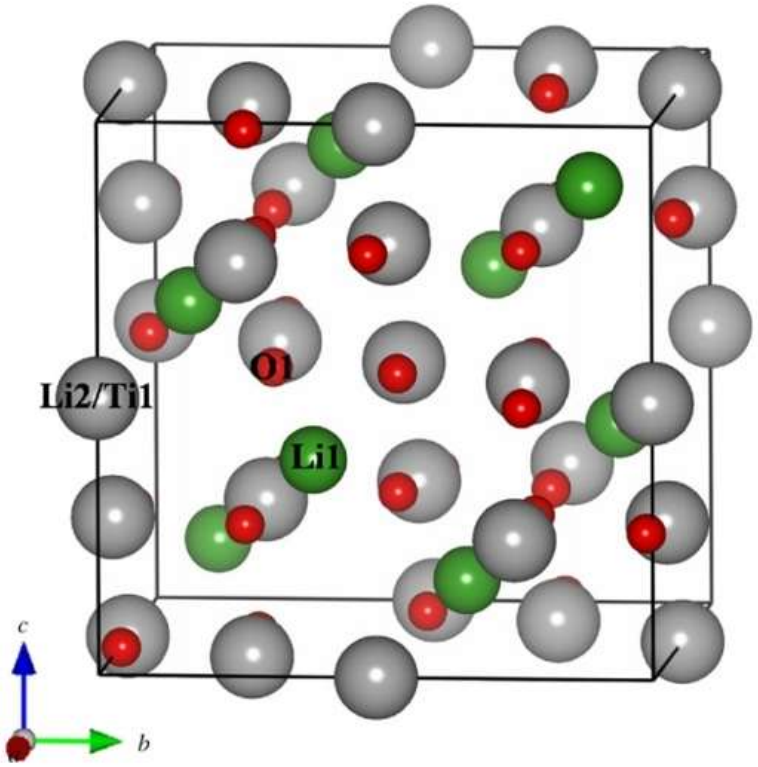

Figure 1.10 Crystal structure of $Li_4Ti_5O_{12}$

The dendritic lithium growth on anode surface at high charging rate has always been the main issue in lithium-ion battery since the conventional carbon based node has almost 0 V vs. Li/Li+ at the end of Li insertion.[15] $Li_4Ti_5O_{12}$ has been proposed as an appealing anode for lithium ion batteries. It's a quite straightforward solution using an electrochemical redox couple with higher equilibrium potentials that can makes Li dendrite less favorable. At 1.56 V, $Li_4Ti_5O_{12}$ inserts three lithium ion per formula unit fulfilling this requirement, with a theoretical capacity of 175 mAh/ g. Also, there's no need to form a SEI layer for certain function which makes this material more promising.

In the spinel $Li_4Ti_5O_{12}$ structure as plotted in figure 1.10. It's a quite stable [Li1/3Ti5/3]16dO4 framework with oxygen atoms take the 32e positions, Ti atoms take 5/6 of the 16d positions and Li atoms take the rest ones. Li atoms occupied the tetrahedral (8a) sites while no atoms take the octahedral (16c) sites. So we denote the structure as [Li]8a[Li1/3Ti5/3]16dO4. Many advantages have been showed comparing by graphite which is currently used. It has a zero-strain insertion (no structure change) during the charge-discharge process which gives an extended cycle life, about 10^4 generally.[16]

Unfortunately, the conductivity of LTO has been an issue since the electronic structure of LTO characterized by empty Ti 3d-states with a band gap energy of 2-3eV makes this material almost an insulator.[17] Due to the regular and tight cubic structure of LTO, diffusion of Li ions is limited. Therefore, the electrochemical properties of $Li_4Ti_5O_{12}$ might not be sufficient for applications like high charging rate/high current.[18] Low capacity of LTO compared to the carbon based anode makes it harder to reach a higher power and energy density.

4. $Li_2Ti_3O_7$ as an anode material for Li-ion batteries

4.1. Introduction

$Li_2Ti_3O_7$ is introduced as an alternative anode material for $Li_4Ti_5O_{12}$. With a ramsdellite structure, $Li_2Ti_3O_7$ allows intercalation and de-intercalation of lithium ions. The reversible intercalation occurs around 1.4 V versus Li/Li+, with a 198 Ah/Kg theoretical capacity. Also, $Li_2Ti_3O_7$ is "a zero-strain" material with a no more than 2% structure change even at high lithium intercalation. The good cycle ability of $Li_2Ti_3O_7$ as an anode material makes it a promising material for potential rock chair batteries. The structure of $Li_2Ti_3O_7$ will be introduced below.

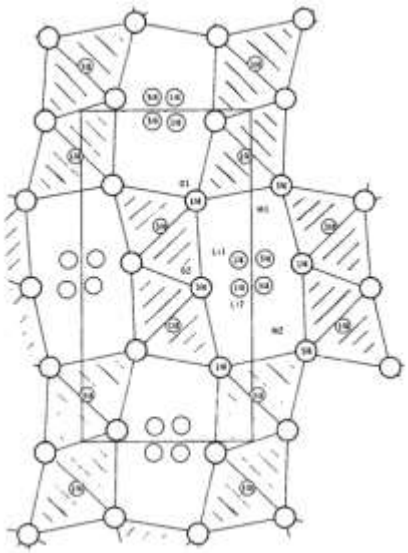

Figure 1.11 A presentation of the structure of $Li_2Ti_3O_7$ along (001) (Adapted from Armand, M. B. in Fast Ion Transport in Solids (ed. Van Gool, W.) 665–673 (North-Holland, Amsterdam, 1973)

$Li_2Ti_3O_7$ was first reported by Jonkers and by Kim some years later with a ramsdellite structure. By sharing the edges, the distorted MO_6 octahedral with adjacent octahedral linked together in the

crystal. The adjacent columns share edges to form double columns which gives an open frame work. There also exist the channels like tunnels right between the double columns.[18-28]

By using single crystal X-ray diffraction (XRD), the location of oxygen and titanium was well established by Morosin and Mikkelsen, which showed us some structure details. The structure Figure consists of TiO_6 octahedra ($Ti_{0.86}Li_{0.14}O_6$ octahedra) with two edge-shared ways: directly above and below forming a string along c, and to an adjacent string displaced ½ along c. The two strings connected together and form a ribbon. In any one channel, there are eight possible tetrahedral sites with four sites of two symmetry sites). Two of them are occupied by Li (1) and Li (2) which are close to the center and the remaining two with a distant sets are located associated with the M1 and M2(the broad, positive value for the electron density). The Ti atoms lies away from the sharing edge because the slightly different of Ti-O distance. The Li+ ions are displaced slightly from the ideal tetrahedral sites and involve a longer and a shorter bond length.[29-31]

The tunnel structure formed by distorted interstitial sites will give the material a nice Li mobility.

5. Purpose of this thesis

$Li_4Ti_5O_{12}$ is a promising material which can be used as anode materials in Li-ion battery to overcome the safety issue. With a long cycle life and calendar life, LTO provide a low cost and simple integration method to achieve high energy density which fulfill the requirement of EVs. But it suffers from low conductivity and low capacity compared to the anode based on carbon.

In this thesis, $Li_4Ti_5O_{12}$-$Li_2Ti_3O_7$ nano composites are synthesized/reprocessed by using rapid thermo processing (RTP) facility. Structures and compositions are deeply investigated, meanwhile, electrochemical properties of regular $Li_4Ti_5O_{12}$ nano powder and new composites are also investigated. In chapter 2, the RTP preparation of the sample which is the synthesize process will be described. In chapter 3 and 4, I will analyze the structure and composition mainly from results, propose possible mechanism of reactions. In chapter 5, I will analyze the electrochemical properties.

Chapter 2 $Li_4Ti_5O_{12}$ sample preparation

1. Process description

RTP machine is a thermo synthesis/process facility which can increase the furnace temperature up to 1200 ℃ within a short time. There is a variety of gas can be chosen to flow through the furnace (Ar, H_2, O_2, etc.). Also, the heating rate and the flow through the furnace of different gas can be micro managed and recorded. It's a quite commonly used machine in all laboratories. We can use RTP machine to do the heat treatment of materials such as annealing. Sometime we find amazing phase chances during/after the thermo process. It's important to note that we can only use silicon as plate and materials which may react with Si at high temperature must be forbidden. Also, mass production of materials cannot be achieved by RTP.

In this thesis, we use RTP machine to synthesis/reprocess $Li_4Ti_5O_{12}$ nano particles at different conditions (gas, temperature and holding time). The processing condition of different samples will be mentioned below.

2. Process design

As showed in figure 2.1, it's an example recipe of RTP process using H_2 as the processing environment. We plot time vs. temperature and marked the type and flow of gas in each part.

The process starts with a high argon flow at 10 (10 is a number defined by the software we use, the maximum is 50, but usually 10 is high enough as a matter of experience) for 300 seconds. The high inert flow is used first to remove the residual gas from last experiments. To make sure the furnace is full of H_2 atmosphere at the start the heating, a 30 seconds H_2 pre-flow (we will also use flow 3 at the rest of this process) comes right after. There is no heating during the last 330 seconds. Then, the heating comes, the temperature of furnace is increased to 800 ℃ in 20 seconds. This time is called ramp time. At 800 ℃, hold the temperature by 300 seconds and this time is called holding time. After the holding, the temperature is decreased in 120 seconds. Last, an argon flow of 150 seconds is added. Wait until the temperature is 50 ℃, the process is done.

It is important that the processing recipes are changed for different processing conditions. E.g., the ramp time varies because there will appear a temperature peak when the temperature is ramped so fast and inaccurate the process. So sometimes we change the ramp time to make sure the holding

process shows a platform in the plot. 0 ℃ in this plot is the room temperature, set the room temperature as 0 ℃ in the system. H_2 refers to 4% H_2 volume concentration at argon atmosphere.

For a particular material, the holding time, ramp temperature and the atmosphere are variables during a RTP processing.

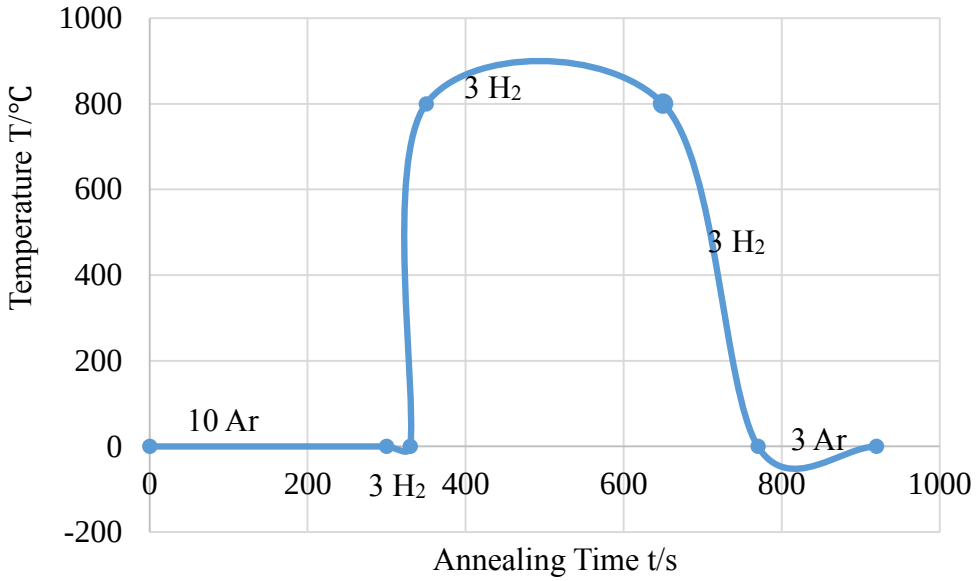

Figure 2.1 Time vs. Temperature in a RTP recipe

Chapter 3 Annealing temperature effect on LTO in RTP processing

1. Stability of LTO at different annealing environments

1.1. Materials preparation

The LTO nanoparticles were first synthesized via a process of nano-spray combustion chemical-vapor condensation, followed by a post-annealing at 800℃ for 3h. First we try to test the stability of LTO at different heating environments to see if there are any phase changes after the processing. Select 800 ℃, 850℃， 900℃ as the annealing temperature, set the hold time as 30 seconds. Also, the reference experiments have been taken at 900℃ for 30 seconds in O_2 and Ar atmosphere.

1.2. Materials characterization

We use X-ray diffraction to identify the phase in each sample. X-ray diffraction patterns of all annealed samples are captured by Rigaku Ultima III X-ray diffractometer. The X-ray source is CuKα, voltage of X-ray cube is 40kV, current in the cube is 44 mA, and scanning step may vary in different measurements to achieve a better XRD result. Several effects may influence the results quality.

1.3 . Stability of LTO at different heating environments

Figure 3.1 shows the powder XRD of sample at 800 ℃. It's a spinel structure with a favorable structure property. There is a small amount of TiO_2 impurity which is agreed with the published paper.

We use different temperature to probe the stability of LTO in H_2. When LTO is annealed at 850 ℃ in H_2 environment with a holding time of 30 seconds, clearly there's a new phase in the sample (Figure 3.2). The phase is identified as $Li_2Ti_3O_7$ after the data analysis using the software Jade. Still, there can be found the TiO_2 impurity. The color of powder turns from white (mainly $Li_4Ti_5O_{12}$) to blue after annealing.

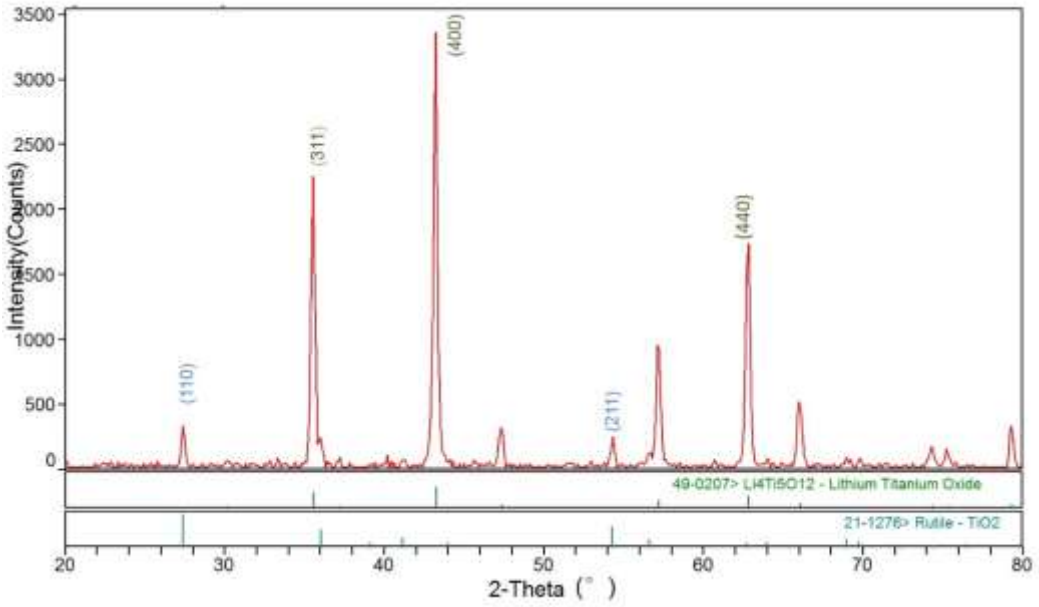

Figure 3.1 XRD pattern of LTO, 30 s H_2 anneal at 800 ℃

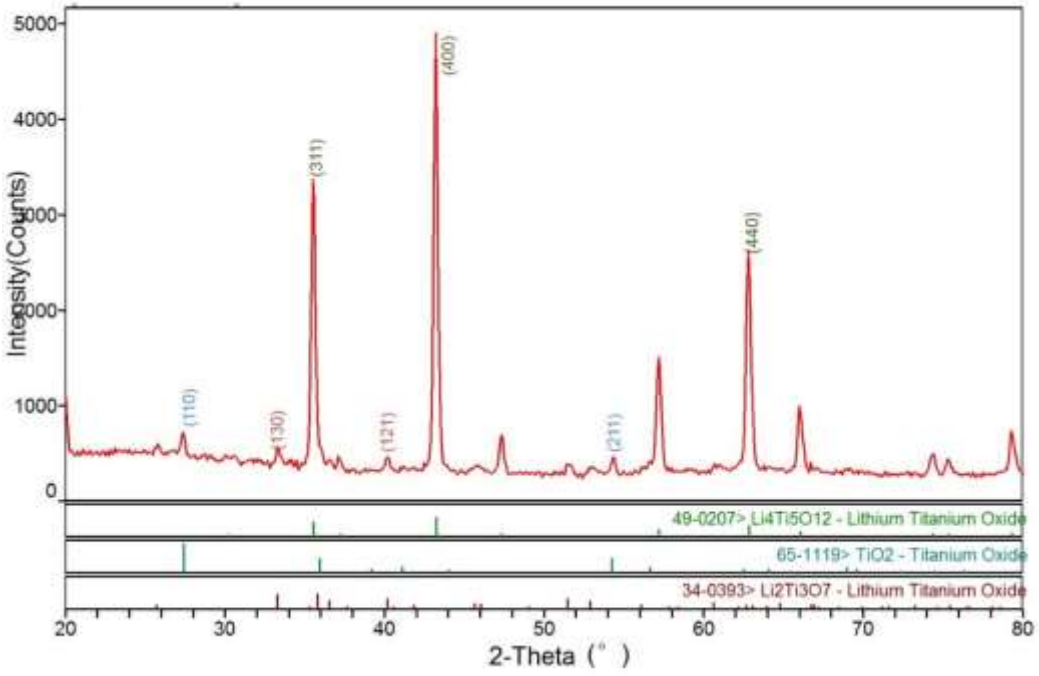

Figure 3.2 XRD pattern of LTO, 30 s H_2 anneal at 850 ℃

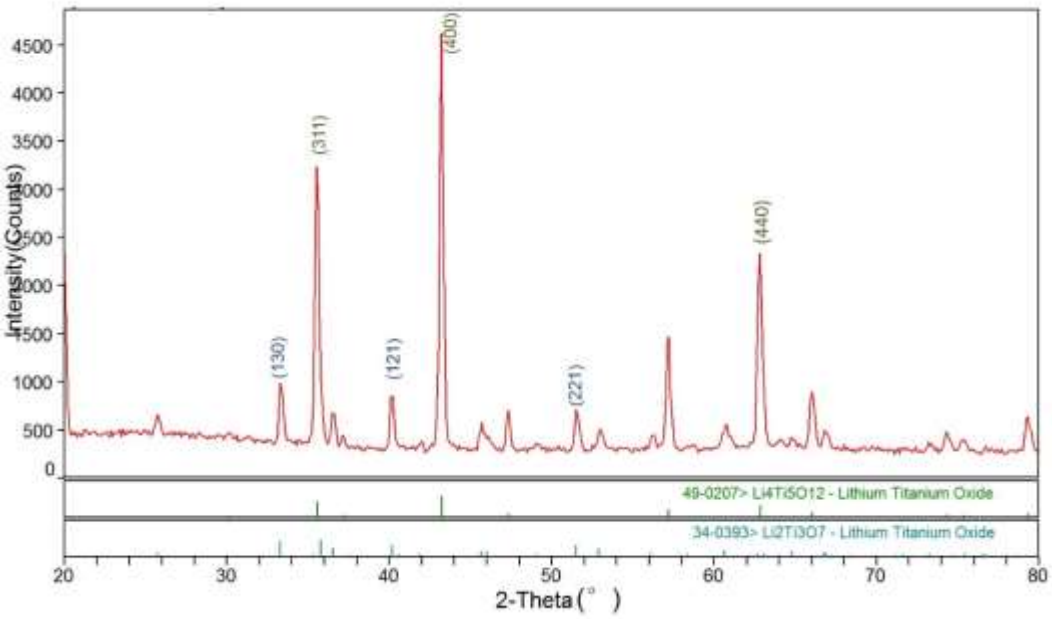

Figure 3.3 XRD pattern of LTO, 30 s H_2 anneal at 900 ℃

Figure 3.3 shows us the XRD of LTO composite when we lift the temperature to 900℃。 Compare this to the last figure, the lattice parameter increase as the Bragg diffraction angle decrease. This is agreed with the increase of $Li_2Ti_3O_7$. There are no clear peaks of TiO_2 which means at this temperature, the TiO_2 has gone. In addition, the color of powder turns to darker blue after annealing.

The exact reaction is still not clear. Here we proposed a reaction mechanism to explain this phenomenon,

$$3Li_4Ti_5O_{12} \leftrightarrow 5\ Li_2Ti_3O_7 + Li_2O$$

It's reasonable to assume $Li_4Ti_5O_{12}$ turns into $Li_2Ti_3O_7$ at the surface of $Li_4Ti_5O_{12}$ nano particles to form a core-shell structure. But it is important to note that during the TEM characterization of material, we haven't got a single HR-TEM image that can prove the core-shell structure. This may because of the asymmetry distribution of particles during the synthesis and TEM sample preparation. Also, lithium is badly damaged under the high energy beams, a phase transformation may occur. Further work needs to be done to identify the "core-shall" assumption.

There are no new phases according to the XRD results of samples annealing at 900℃ for 30 seconds in O_2 and Ar. (Figure 3.4 and 3.5)

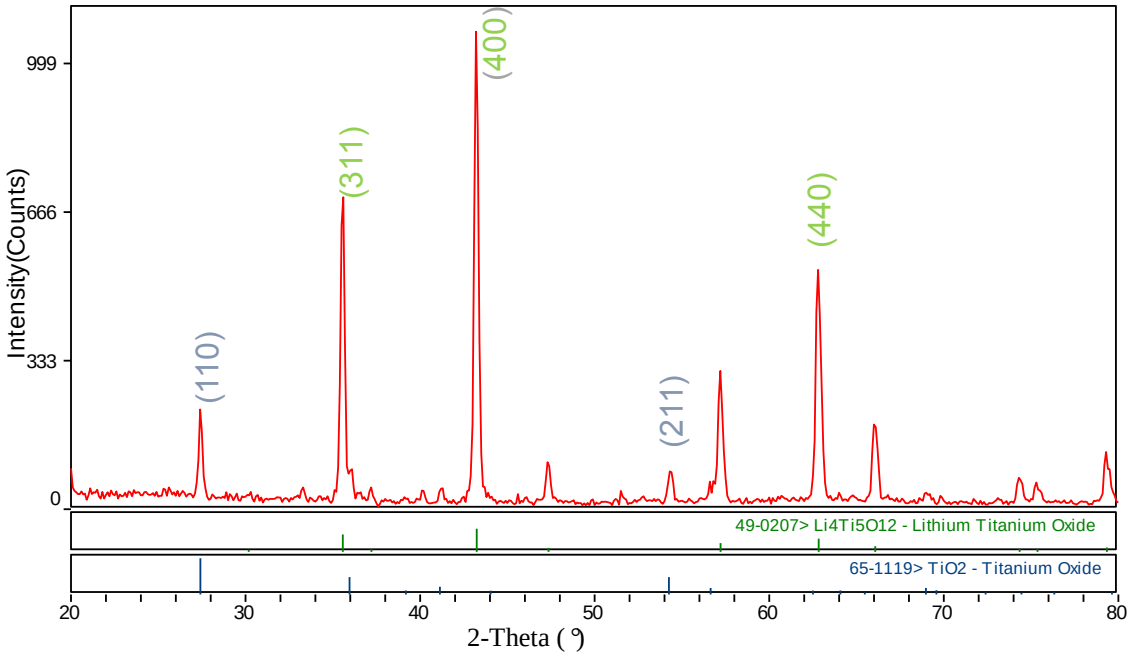

Figure 3.4 XRD pattern of LTO, 30 s O_2 anneal at 900 ℃

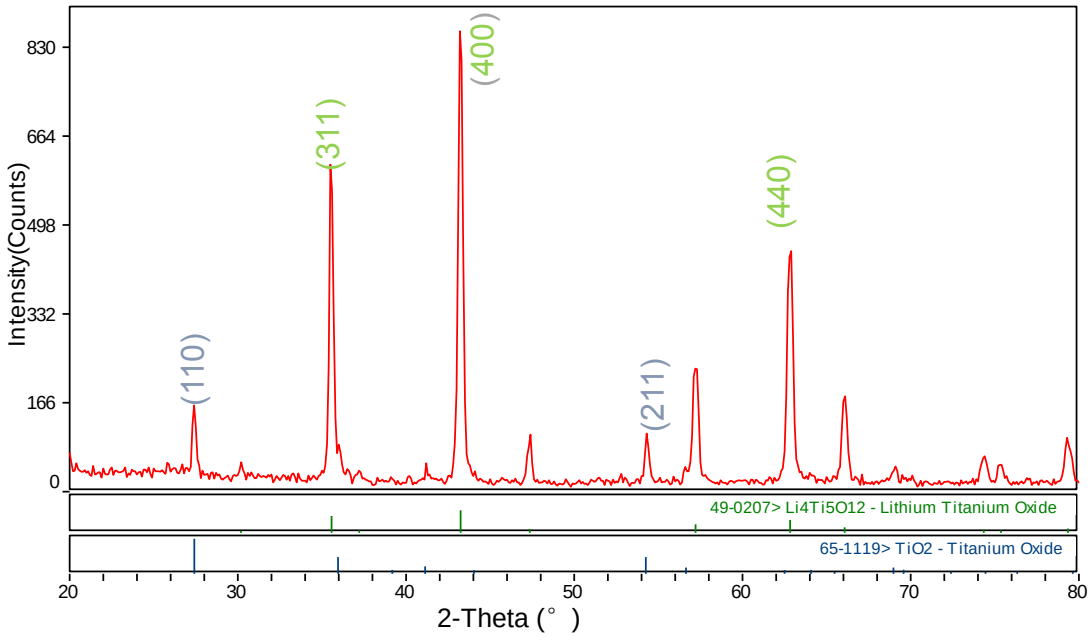

Figure 3.5 XRD pattern of LTO, 30 s Ar anneal at 900℃

2. Annealing temperature effect on LTO in RTP processing

2.1. Materials preparation

After knowing at 850 ℃, there is a phase transition from spinel to ramsdellite, i.e. $Li_4Ti_5O_{12}$ to $Li_2Ti_3O_7$, we researched on annealing temperature effect on LTO in RTP processing. Select 800 ℃, 825 ℃, 850 ℃, 875 ℃, as the annealing temperature, set the hold time as 60 seconds, and name the sample as 800-60, 825-60, 850-60, and 875-60 respectively.

2.2. Materials characterization

We use X-ray diffraction to identify the phase in each sample. X-ray diffraction patterns of all annealed samples are captured by Rigaku Ultima III X-ray diffractometer. The X-ray source is CuKα, voltage of X-ray cube is 40kV, current in the cube is 44 mA, and scanning step may vary in different measurements to achieve a better XRD result. Several effects may influence the results quality.

The TEM measurements are conducted on JEOL-2100F. It's a 120-200kV scanning transmission and transmission field-emission electron microscope (STEM/TEM) for high-resolution analytical structural characterization. It is equipped with a chottky field-emission gun and two exchangeable objective-lens pole-pieces (an ultra-high-resolution pole-piece with a 0.19 nm point-to-point resolution and a ±20 ° sample tilt, and a high-resolution pole-piece with a 0.23 nm point-to-point resolution and a ±40 ° sample tilt). The instrument is also equipped with an energy dispersive x-ray spectrometer for chemical analysis, and heating and cooling stages for in-situ experiments and dynamic observations. We mainly use TEM mode to conduct all the experiments on this research to take HR-TEM images and diffraction patterns.

2.3. XRD study

Figure 3.6, 3.7, 3.8, 3.9 show us the powder XRD results of 800-60, 825-60, 850-60, and 875-60 respectively.

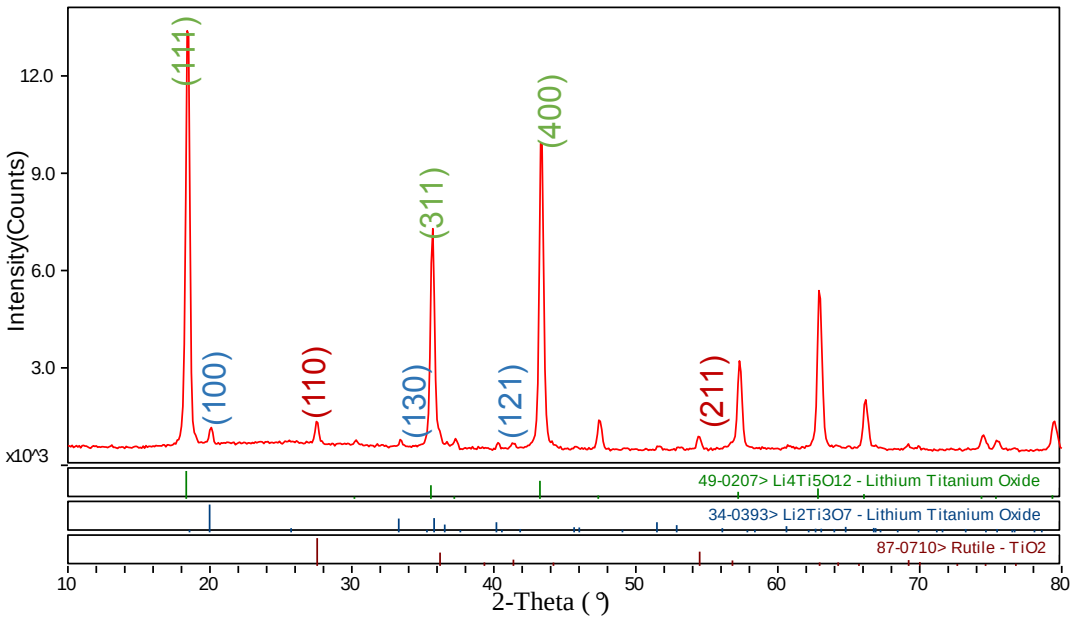

Figure 3.6 XRD pattern of LTO, 60 s H_2 anneal at 800 ℃

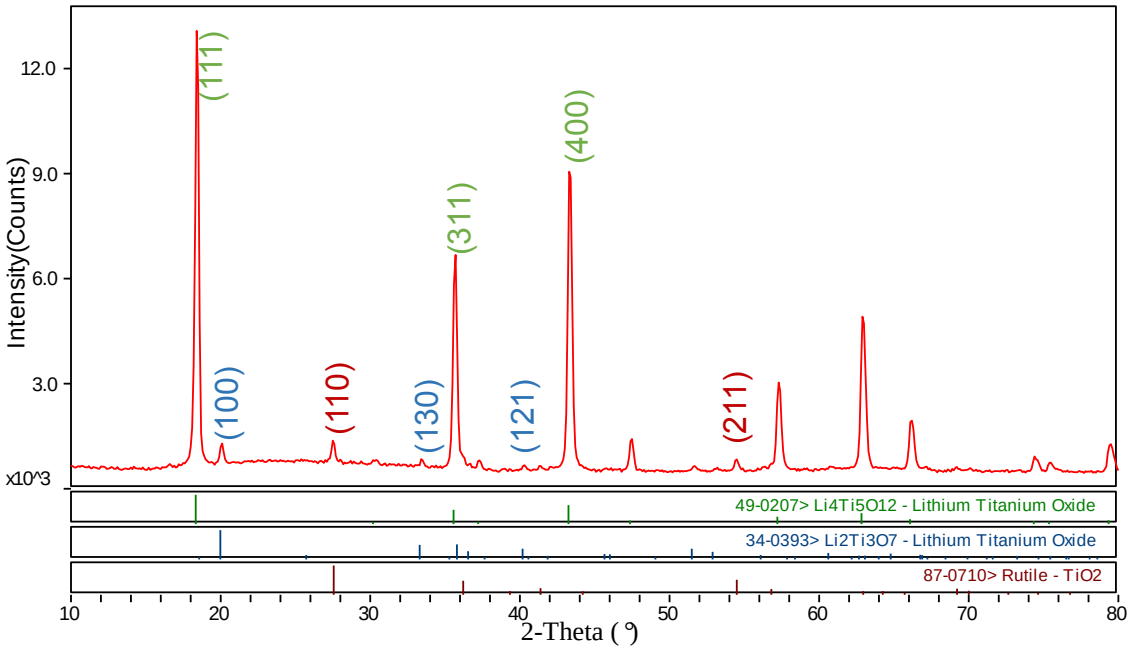

Figure 3.7 XRD pattern of LTO, 60 s H_2 anneal at 825 ℃

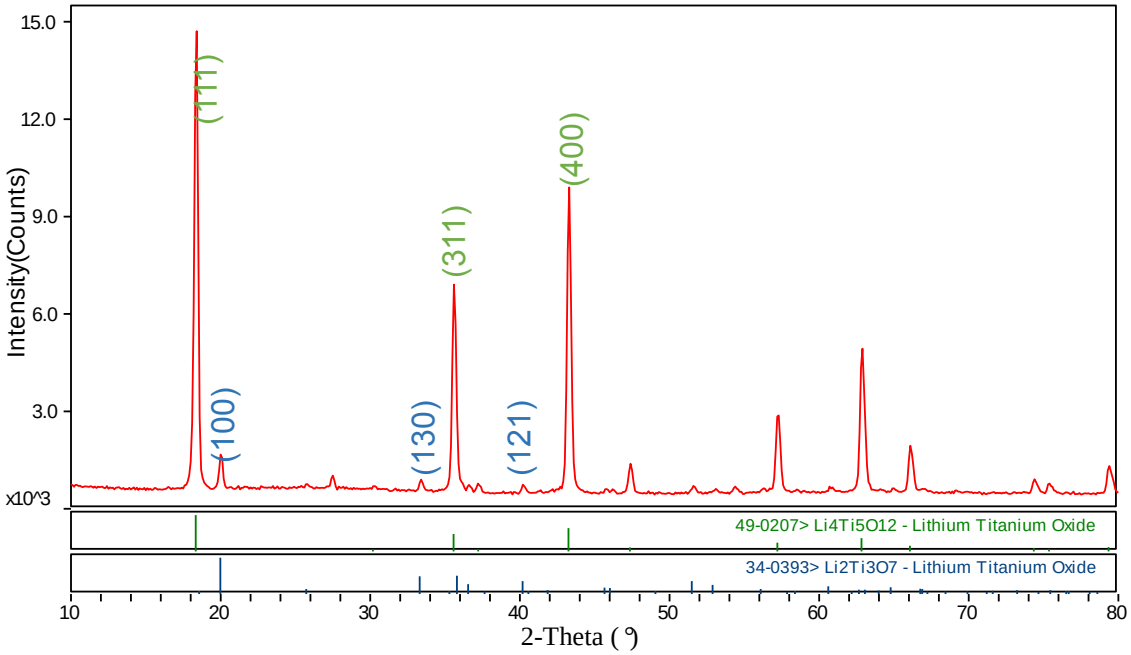

Figure 3.8 XRD pattern of LTO, 60 s H_2 anneal at 850 ℃

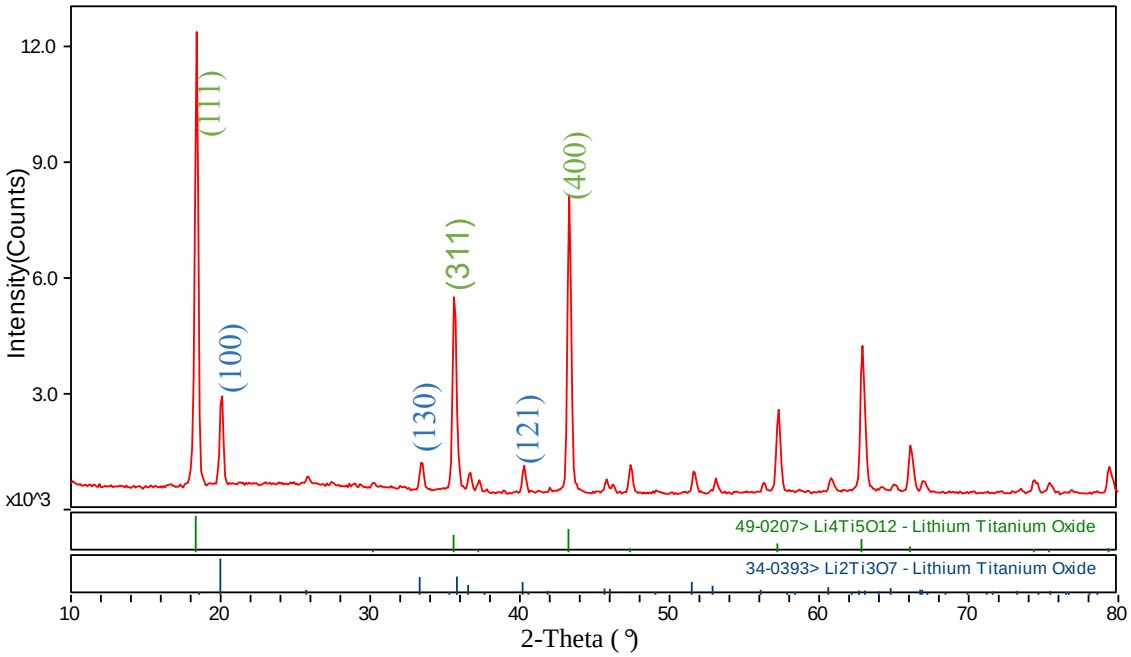

Figure 3.9 XRD pattern of LTO, 60 s H_2 anneal at 875 ℃

The lattice parameter increase as the Bragg diffraction angle decrease when we increase the annealing temperature. This is agreed with the half-quantitate calculation results that the $Li_2Ti_3O_7$ increase as the annealing temperature increase which we will mention below.

2.4. Half-quantitate calculation

Since 1978, the PDF card published by ICDD have the RIR value attached. It's ratio of the highest integrated intensity of a sample material and a reference material. As showed in equation 3-1

$$RIR = I_i / I_{col} \tag{3-1}$$

In this equation, I_i and I_{col} are integrated intensity of phase i and the reference (Usually we use α-Al_2O_3 as a reference material). According to the adiabatic approximation method, if there are N phases in a system, the mass percentage of the phase I can be described by the RIR value of each phase. As showed in equation 3-2

$$W_i = \frac{I_i}{RIR_i} / \sum_{i=1}^{N} I_i/RIR_i \tag{3-2}$$

The intensity of peaks in XRD varies due to different reasons and then the RIR value varies a lot. The changing of chemical components, powder granularity, and particle size, crystal structure of alloys and environment of experiments may influence the results we have. Peak width and shape are also different in XRD of different components. That's why we say it's a half-quantitate analysis. For an accurate XRD measurement, the relative error of mass percentage based on RIR calculation can be controlled only up to 5%. For a continuous XRD measurement of phase identification, relative error may up to 10%. In our measurement, we introduce one more way to calculate the volume percentage and do both of the calculation to reduce the relative error, hope to see a clearly trend of $Li_2Ti_3O_7$in different processing environment.

$$V_i = \frac{\frac{1}{n}\sum_{j=1}^{n}\frac{I_i^j}{R_i^j}}{\sum_j \frac{1}{n}\sum_{j=1}^{n}\frac{I_i^j}{R_i^j}} \tag{3.3}$$

In this equation, I_i^j is integrated intensity, R_i^j is I% (relative intensity) of each peak which we can find from the XRD peak report. The equation is also based on adiabatic approximation method but using R_i^j instead of RIR.

Since there are so many peaks of each component in a XRD, we only select data of the highest 3 peaks to do each calculation. RIR value of each component has been looked up in PDF cards. To be more clarified, not only we calculated the fraction of each component, the fraction ratio of $Li_2Ti_3O_7$ and $Li_4Ti_5O_{12}$ has been calculated and plotted (including mass and volume percentage).

Figure 3.10, 3.11 are half-quantitate calculation results of XRD. We plot the annealing temperature vs. M%-$Li_2Ti_3O_7$/M%-$L_4Ti_5O_{12}$ at 800 ℃, 825 ℃, 850 ℃ and 875℃. The mass percentage ratio start from 0.040% with a composition of 0.038% $Li_2Ti_3O_7$ and 0.935% at 800℃. The ratio then increase slowly to 0.046% and 0.080% at 825℃ and 850℃. A huge increase come after at 875℃. The final composition is 0.168% $Li_2Ti_3O_7$ and 0.832% $L_4Ti_5O_{12}$.

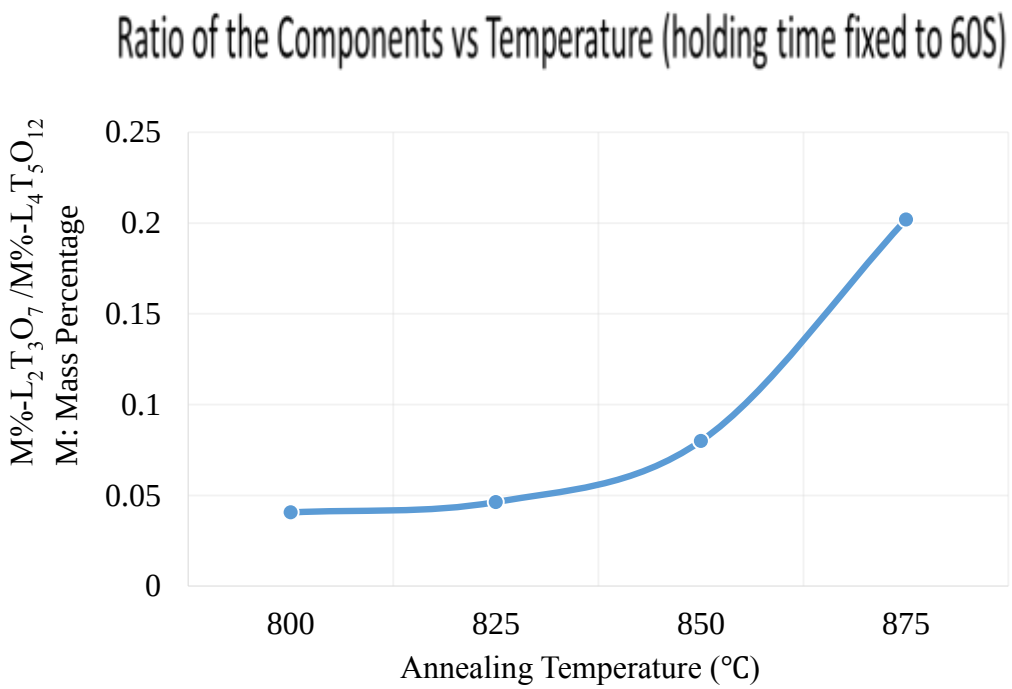

Figure 3.10 Half-quantitate calculation results from the XRD data of different LTO samples. Annealing temperature vs. M%-$Li_2Ti_3O_7$/M%-$L_4Ti_5O_{12}$ (M: mass percentage)

The impurity phase $Li_2Ti_3O_7$ increases as the annealing temperature increases. At 875℃ with 60 seconds annealing, the composite has the highest amount of $Li_2Ti_3O_7$. To be noticed, the TiO_2

still exist at 800 ℃, 825 ℃ annealing temperature but it has gone when the temperature is 850 ℃ and 875℃ (This is showed in previous XRD data).

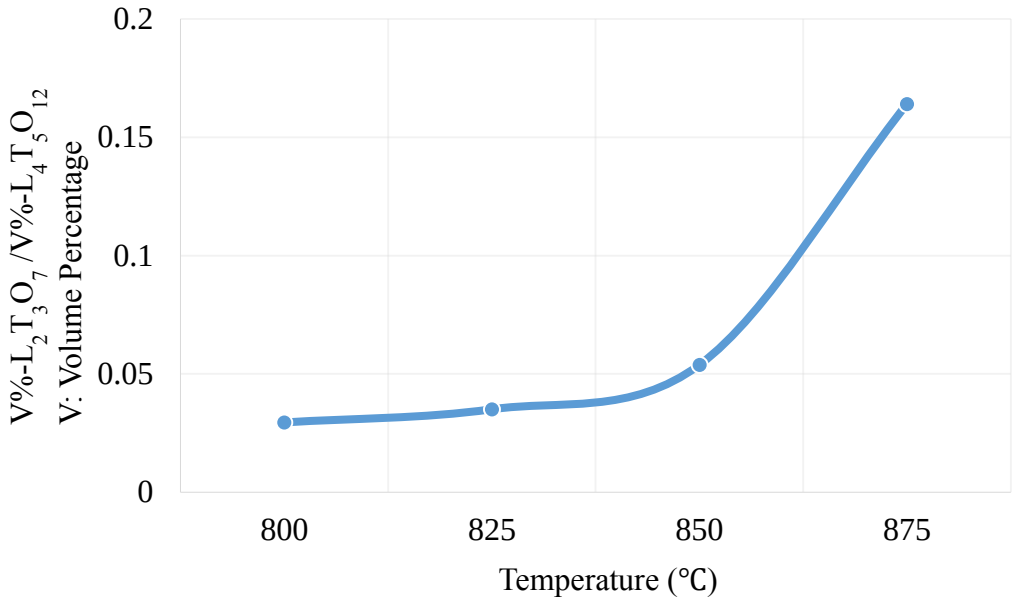

Figure 3.11 Half-quantitate calculation results from the XRD data of different LTO samples. Annealing temperature vs. V%-$Li_2Ti_3O_7$/V%-$L_4Ti_5O_{12}$ (V: volume percentage)

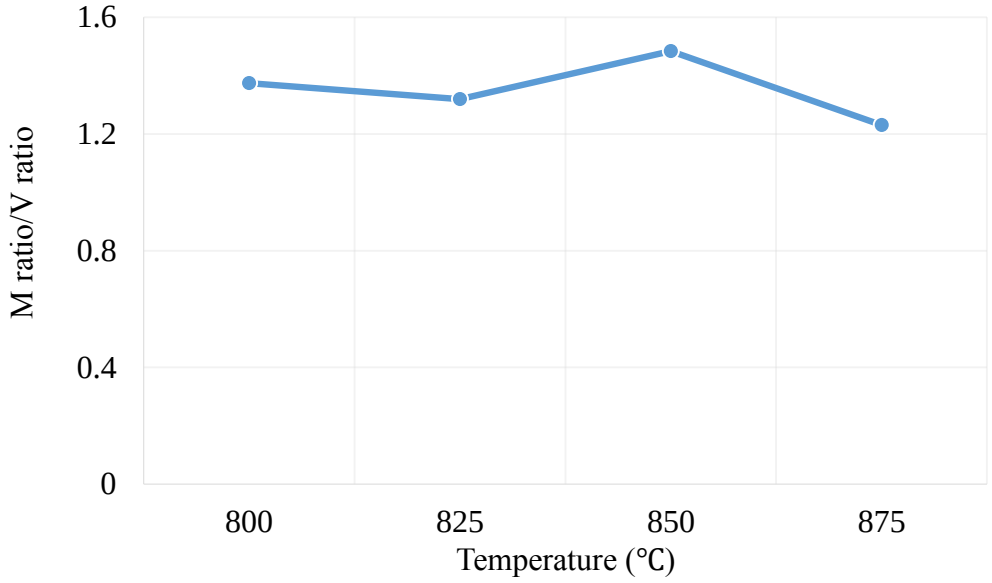

Figure 3.12 M ratio/V ratio vs. annealing time (Samples were annealed at 800 ℃, 825 ℃, 850 ℃ and 875 ℃ respectively)

2.4. TEM study

Figure 3.13 is the bright field image of sample 875-60. This low mag image shows the particles of sample have a rectangle shape with a 30-40nm length which is agreed with published papers. Figure 3.14 is the HR-TEM image of a particle. Figure 3.15 is SAED pattern of area showed in figure 3.14. It's a $Li_2Ti_3O_7$ particle lies along the <110> direction. The results are highly agreed with the previous XRD measurement.

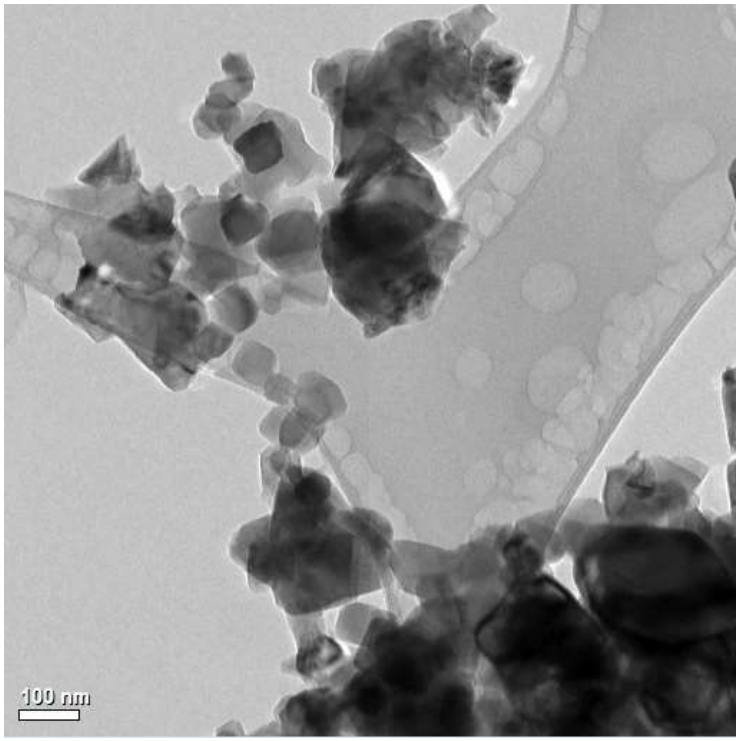

Figure 3.13 Bright field image of LTO, 60 s H_2 anneal at 875 ℃

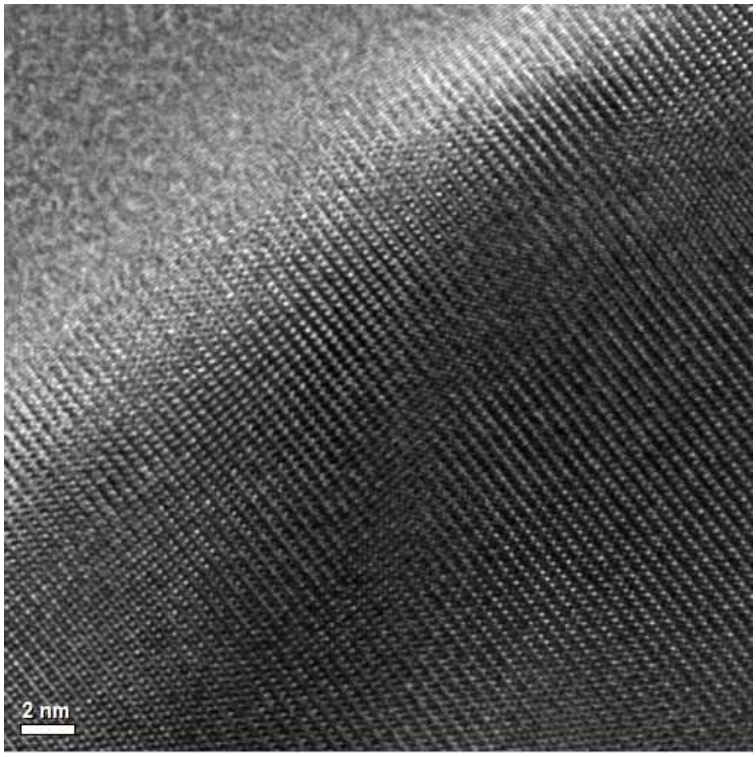

Figure 3.14 HR-TEM image of LTO, 60 s H_2 anneal at 825 ℃

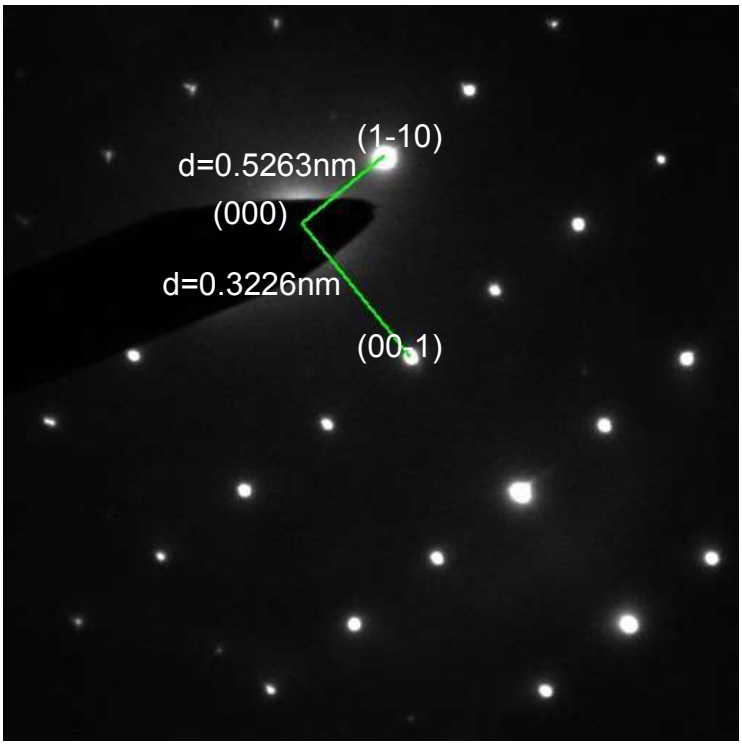

Figure 3.15 SAED along <110> direction of LTO, 60 s H_2 anneal at 825 ℃

Chapter 4 Optimization of LTO-RLTO composite

1. Sample preparation

The idea of this experiment came out because of the previous research on temperature effect. Since at 850 ℃, there is a phase transition from spinel to ramsdellite, i.e. $Li_4Ti_5O_{12}$ to $Li_2Ti_3O_7$, it's a quite straight forward idea to research on the effect of holding time and then optimize the LTO-RLTO composite. Select 880 ℃, 900℃ as the annealing temperature, set the hold time as 5, 10, 30, 60, 120 seconds, and name the sample as 880-5, 880-10, 880-30, 880-60, 880-120 and 900-10, 900-30, 900-60, 900-120 respectively.

2. Materials characterization

Still, we mainly use X-ray diffraction to identify the phase in each sample. X-ray diffraction patterns of all annealed samples are captured by Rigaku Ultima III X-ray diffractometer. The X-ray source is CuKα, voltage of X-ray cube is 40kV, current in the cube is 44 mA, scanning step may vary in different measurements to achieve a better XRD result and the scanning range is 10 ° to 80 °in each experiment. Several effects may influence the results quality.

The XRD data which we use for quantitate calculation are analyzed by Jade.

3. Holding time effect on LTO in RTP processing

Figure 4.1 and 4.2 show us the powder XRD of 880-10 and 880-30. They both contain $Li_4Ti_5O_{12}$, $Li_2Ti_3O_7$ and TiO_2.

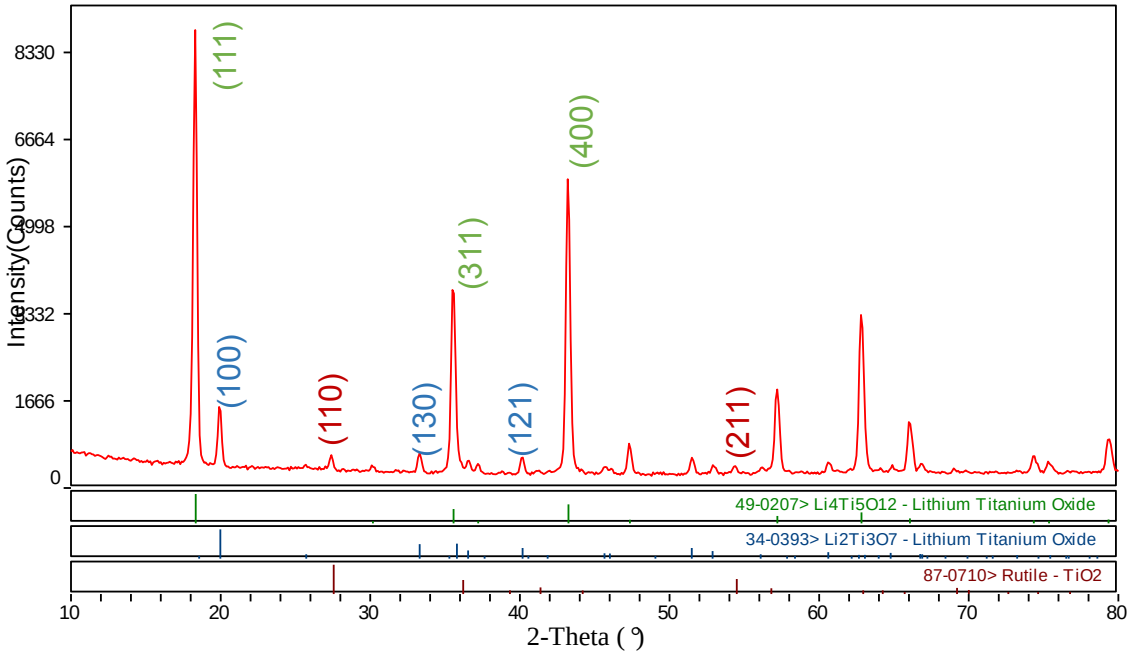

Figure 4.1 XRD pattern of LTO, 10 s H_2 anneal at 880 ℃

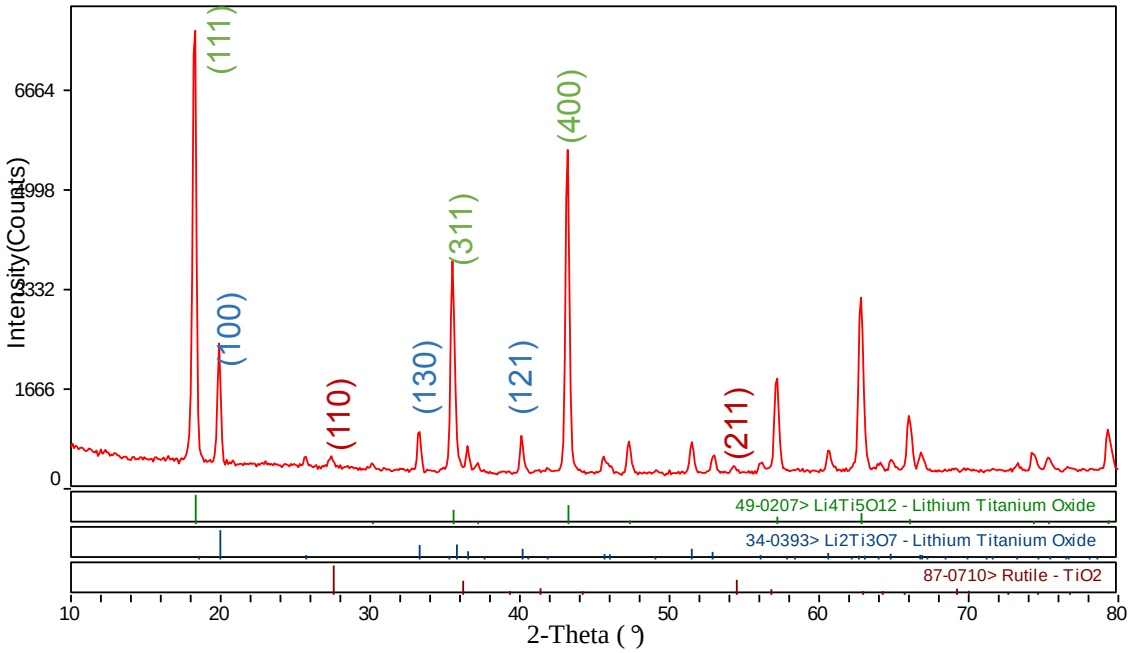

Figure 4.2 XRD pattern of LTO, 30 s H_2 anneal at 880 ℃

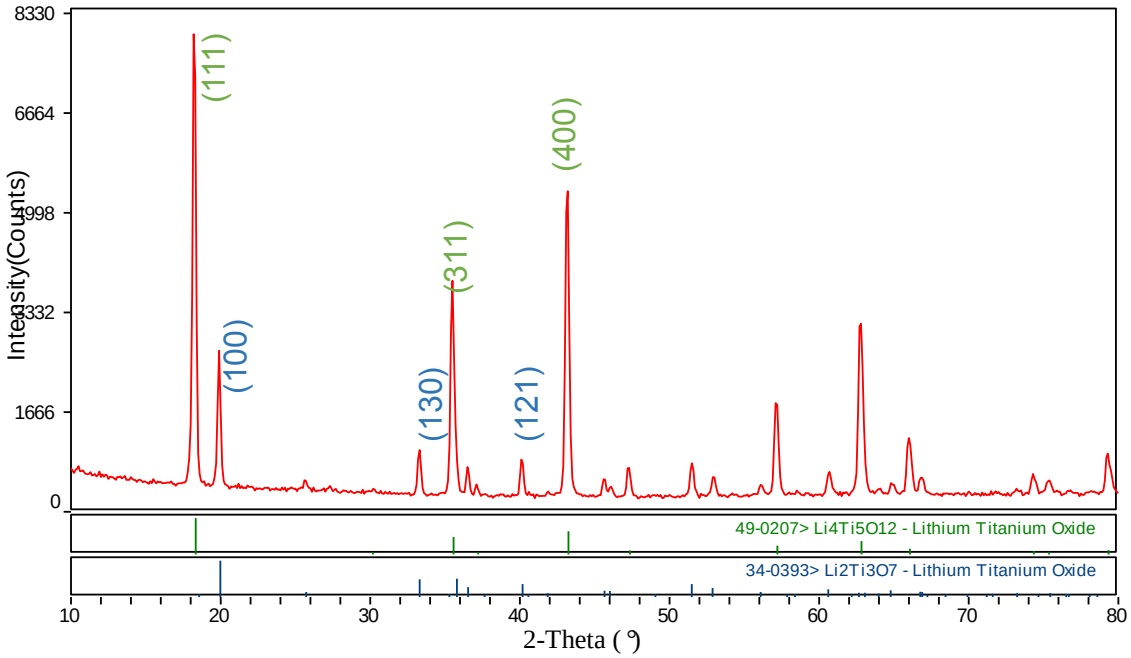

Figure 4.3 XRD pattern of LTO, 60 s H_2 anneal at 880 ℃

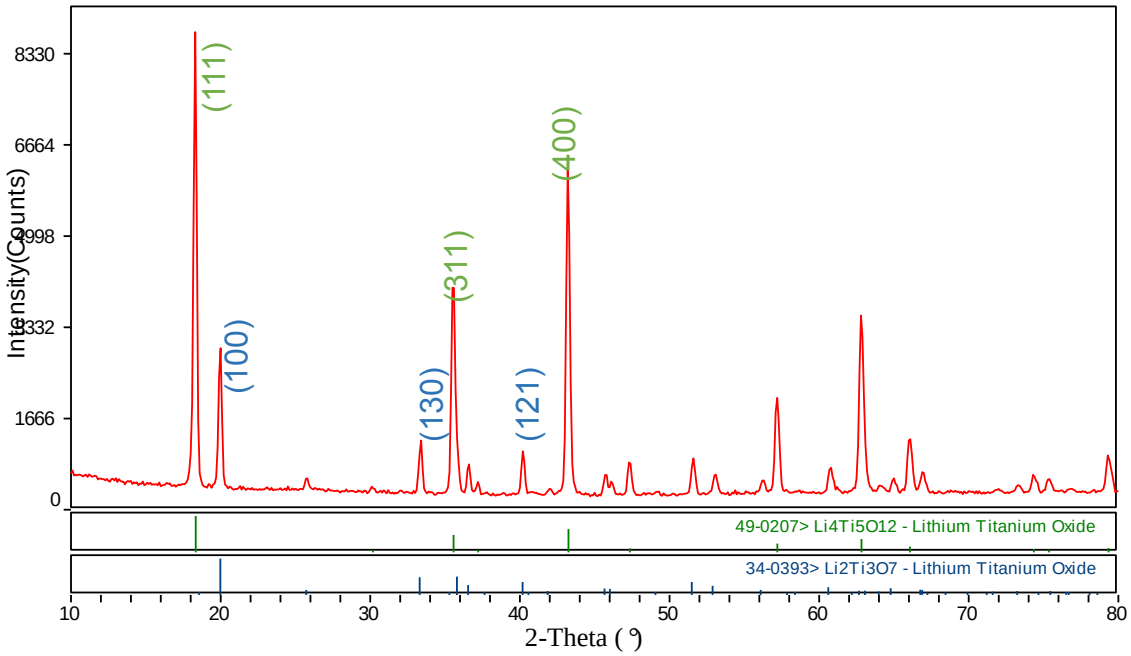

Figure 4.4 XRD pattern of LTO, 120 s H_2 anneal at 880 ℃

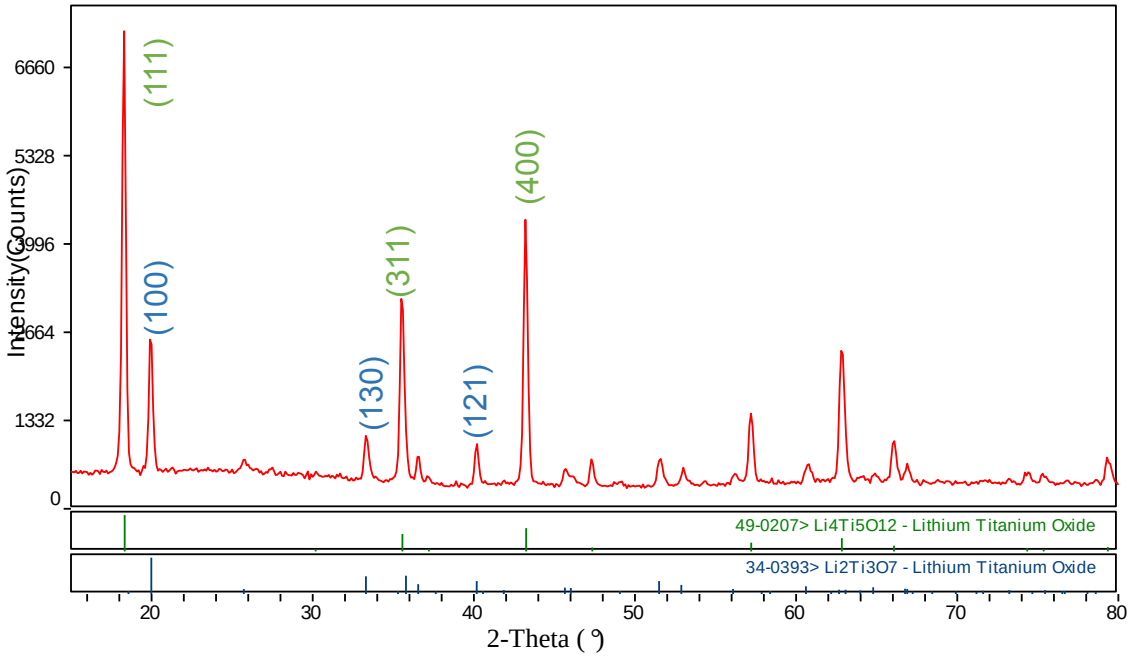

Figure 4.5 XRD pattern of LTO, 10 s H_2 anneal at 900 ℃

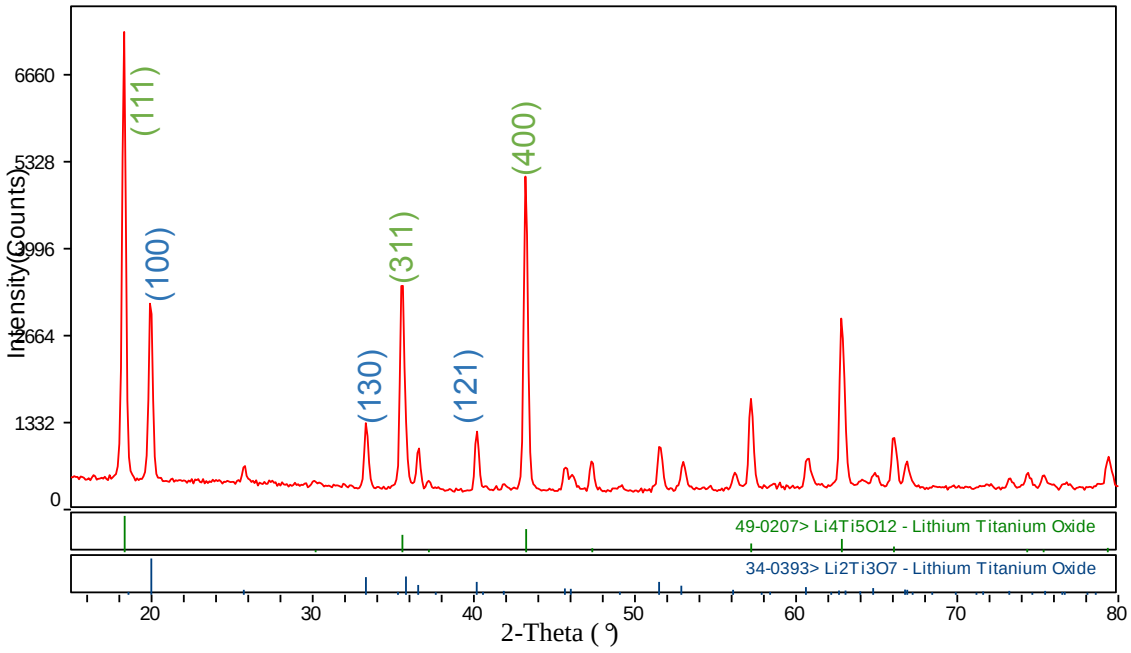

Figure 4.6 XRD pattern of LTO, 30 s H_2 anneal at 900 ℃

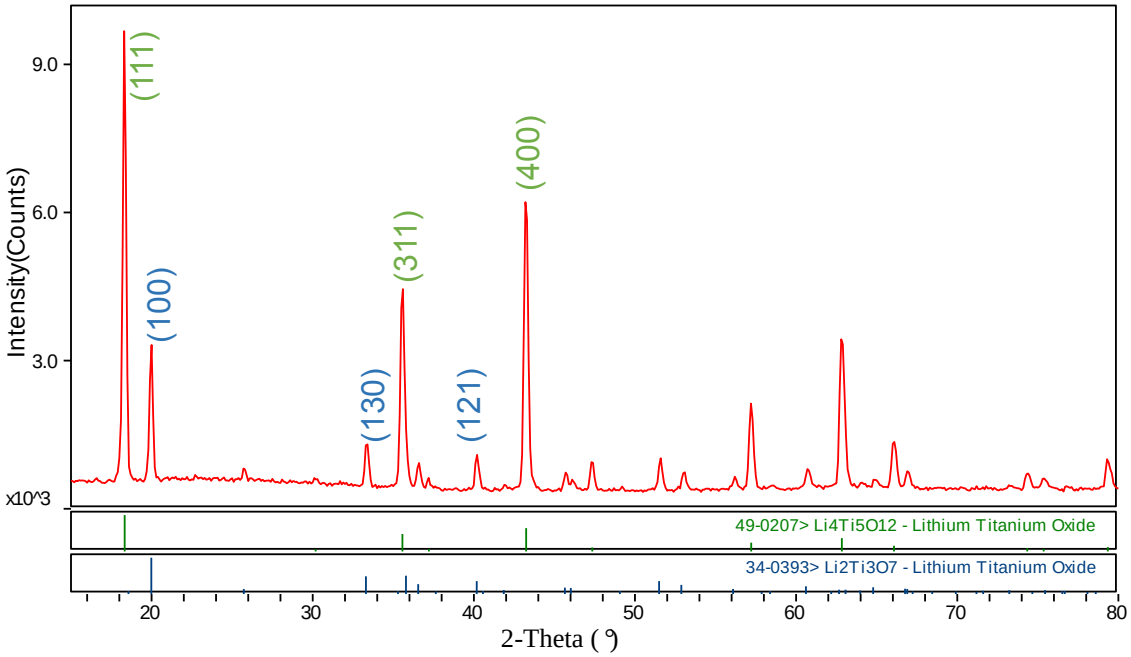

Figure 4.7 XRD pattern of LTO, 60 s H_2 anneal at 900 ℃

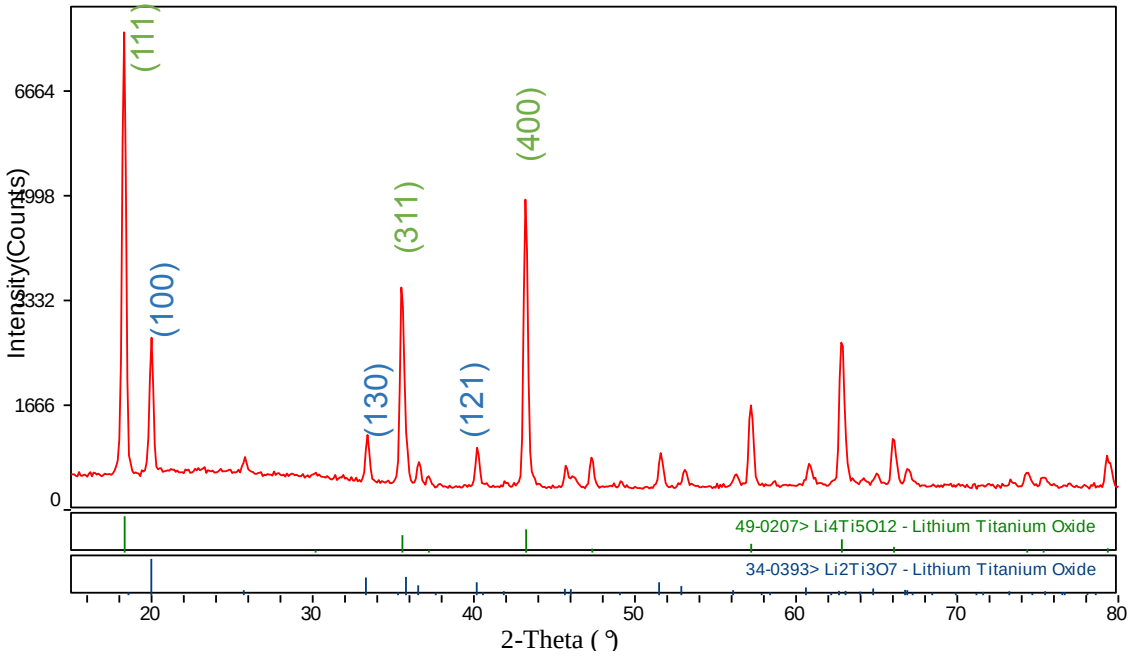

Figure 4.8 XRD pattern of LTO, 120 s H_2 anneal at 900 ℃

Figure 4.3, 4.4, 4.5, 4.6, 4.7, 4.8 show the powder XRD of 880-60, 880-120 and 900-10, 900-30, 900-60, 900-120 respectively. Each sample shows a composite with $Li_4Ti_5O_{12}$ and $Li_2Ti_3O_7$. The lattice parameter increase as the Bragg diffraction angle decrease when we increase the annealing holding time. This is also agreed with the increase of $Li_2Ti_3O_7$.

Further results of half-quantitate based on XRD results will be talked below.

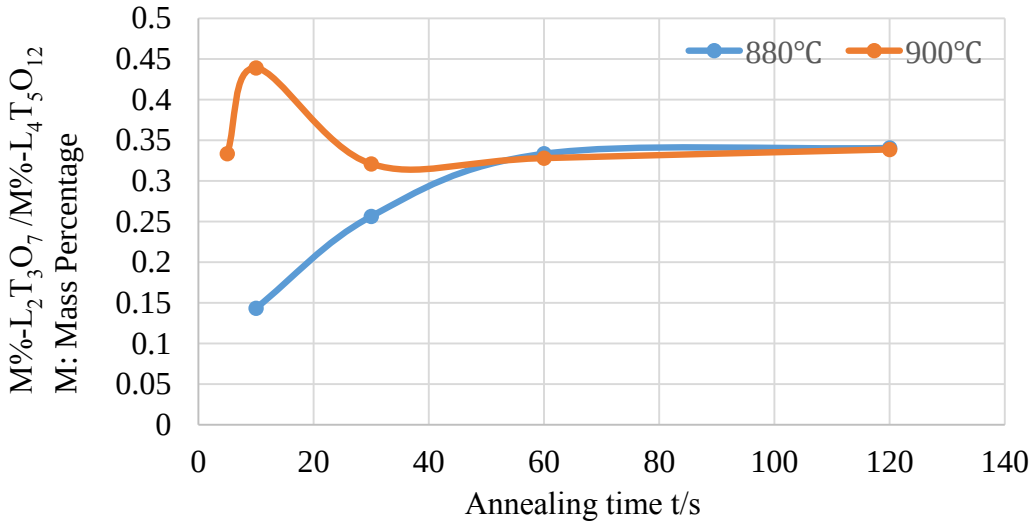

Figure 4.9 Half-quantitate calculation results from the XRD data of different LTO samples. Annealing time vs. M%-$Li_2Ti_3O_7$/M%-$L_4Ti_5O_{12}$ (M: mass percentage)

As is shown above, we plot the annealing holding time vs. M%- $Li_2Ti_3O_7$ /M%- $Li_4Ti_5O_{12}$ at 880 ℃ and 900 ℃, the mass percentage M%- $Li_2Ti_3O_7$ /M%- $Li_4Ti_5O_{12}$ start with 0.143 % at annealing holding time of 10 seconds, and follow up with an increase to 0.256%. The increase of mass percentage keep going as the holding time keep increasing. A plateau shows after the holding time reaches 60 seconds.

It's quite clearly the impurity phase of $Li_2Ti_3O_7$ increases as the holding time increases. The phase composition becomes relatively stable at 60 seconds holding time with a final mass percentage of $Li_2Ti_3O_7$ and $Li_4Ti_5O_{12}$ being as 25.4%and 74.6%, respectively. To be noticed, the TiO_2 still exist at 10 seconds, 30 seconds holding time but it has gone when we increase the holding time to 60 seconds as we've mentioned above

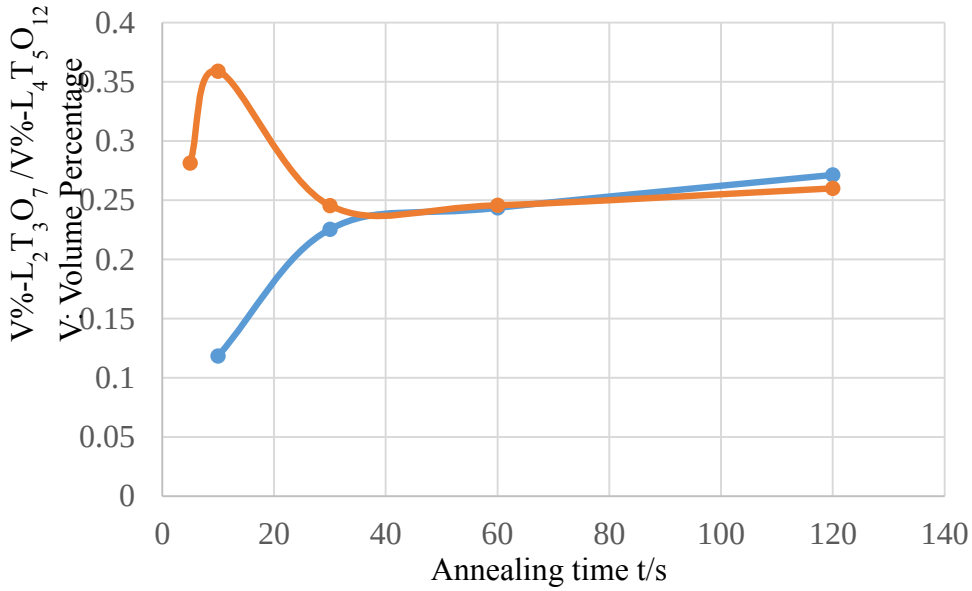

Figure 4.10 Half-quantitate calculation results from the XRD data of different LTO samples. Annealing temperature vs. V%-$Li_2Ti_3O_7$/V%-$L_4Ti_5O_{12}$ (V: volume percentage)

At 900 ℃ the mass percentage start with 0.333% at annealing holding time of 5 seconds, followed up with a huge increase to 0.439% at annealing holding time of 10 seconds. And then the mass percentage drop to 0.321% at 30 seconds with a plateau following up at 60 seconds and 120 seconds.

Since there might be errors occur during the XRD measurement, we disregard the huge increase from 0.333% to 0.439%. Then the line of mass percentage at 900 ℃ shows approximately flat which means the structure and component at 900 ℃ reach to a stable state no matter how we change the holding time. Also, at this annealing temperature, no TiO_2 has been found.

Figure 4.10 shows the plot of annealing holding time vs. V%-$Li_2Ti_3O_7$/V%-$Li_4Ti_5O_{12}$. After comparing the two lines, after both of them reach the plateau, the phase composition (including the variety and the mass percentage of each phase) are approximately the same. This shows a final state of LTO using rapid thermo annealing as a synthesis/reprocessing method can be reached when annealing temperature is higher than 900 ℃ or the holding time ≥ 60 seconds at 880 ℃, with a result of a composition with 25.4% $Li_2Ti_3O_7$ and 74.6% $Li_4Ti_5O_{12}$.

When we double check the figure of volume percentage, the results we have is highly agreed with the previous result using the half-quantitate calculation of mass percentage. There is also a huge increase of volume percentage when the holding time changes from 5 seconds and 10 seconds. The plateaus of both lines appear at the same range of temperature as we showed in previous figure.

Finally, we check the relative error by dividing the mass percentage by the volume percentage since Mass/Volume=Density, the result should be a constant. As is showed in figure 4.11, the fitting lines both are straight with a relative error < 10% at 880 ℃ and 900 ℃. The result is acceptable.

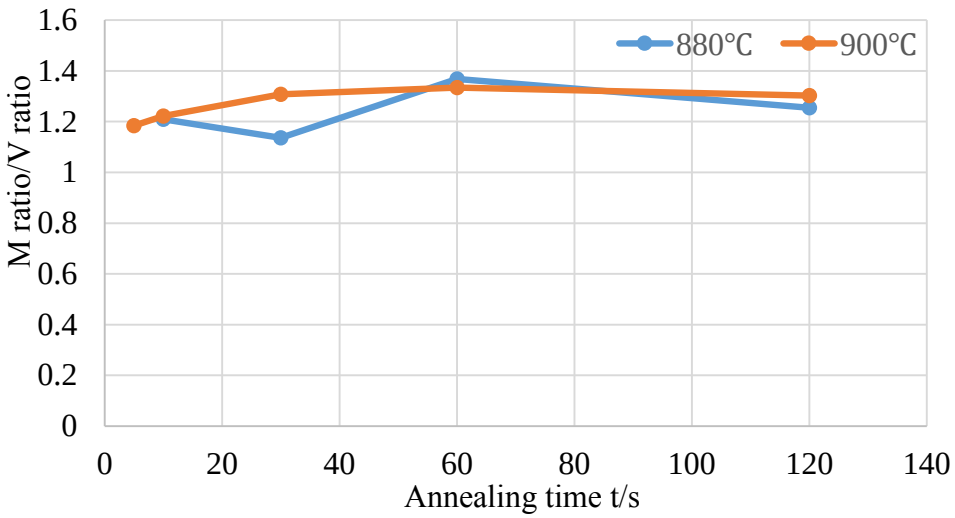

Figure 4.11 M ratio/V ratio vs. annealing time (Samples were annealed at 880 ℃ and 900 ℃ respectively)

Chapter 5 Electrochemical study

1. Introduction

In laboratories, we usually use coin cell to measure the electrochemical properties. It's a simple and easy way to assemble lithium ion cells.

During electrochemical study, we did charging-discharging tests to have charging-discharging curves and cycle life properties, also there are CV and AC impedance test to evaluate different properties of a cell and the materials we use. For some reasons, we only use the charging-discharging test in this thesis to study the properties of cell made by annealed samples.

2. Coin cell assemble

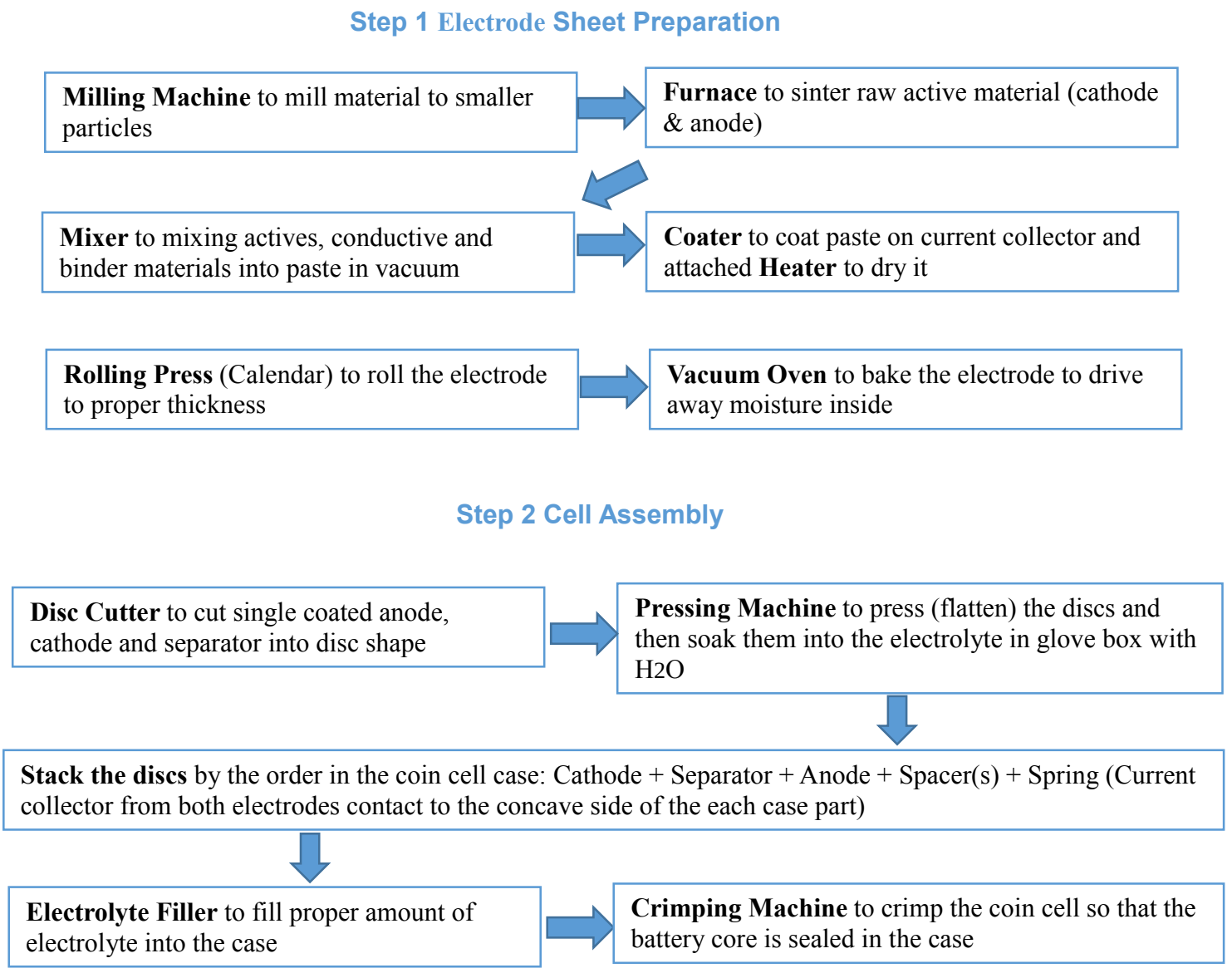

Figure 5.1 The Li-ion coin cell assemble

The Li-ion coin cell assemble is showed above.

3. Electrochemical study

The current during the charging-discharging process is 0.17*m*n (mA) (Assume there are mg material in anode, use nC as the charging-discharging rate). Using 0.2C rate test the sample 875-60 and the regular LTO, plot the capacity vs. voltage of 40th cycle and cycle number vs. capacity. The theoretical capacity of LTO is 170 mAh/g. We can estimate the capacity and mass of the electrode by current and step time according to the data. For example, if the discharge finished in 4.5h, the capacity of the material is 170*(4.5/5) = 153 mAh g^{-1}, but there will be experimental errors.

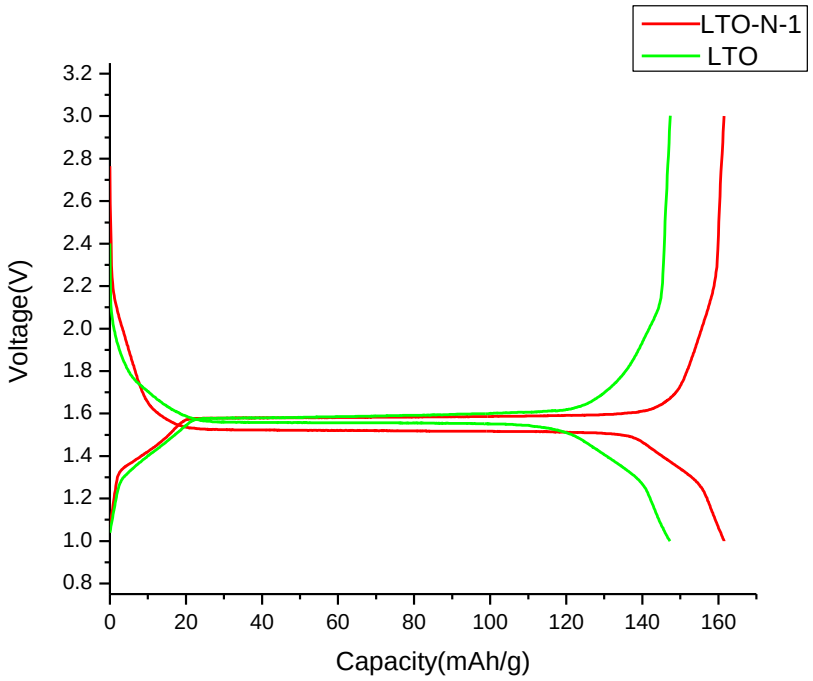

Figure 5.2 Cycling performance of Li-ion intercalation-deintercalation reactions for the LTO samples

As shown in figure 5.2 above, it's the cycling performance of LTO samples at 40th cycle. LTO is the regular $Li_4Ti_5O_{12}$ and LTO-N-1 is LTO with 60 s H_2 anneal at 875 ℃.The open circuit voltage is 2.8 V which is always less than the theoretical voltage. During the discharge process, LTO has a plateau occur at 1.5V which is highly agreed with published papers. Also, LTO has a cutting voltage of 1V same as the LTO-N-1 sample.

If we compare the plots of two materials, the LTO-N-1 has a capacity increase from 150m Ah/g to 162m Ah/g. This is due to the increase of $Li_2Ti_3O_7$ structure. The tunnel structure can accept more Li ions which shows a better result of capacity. But the working potential difference between

charging and discharging is bigger than the LTO, i.e. voltage efficiency is smaller (The charging plateau is always higher than the discharging plateau because the electron kinetics is sluggish. We can't avoid over potentials, current flowing and omega potential differences.). Some batteries may have a huge difference like 1V.

Also, materials which have a voltage plateau during charging and discharging can provide a stable working voltage. But it's impossible to track the battery level. That's why people choose different materials for lithium ion battery to reach different purposes.

The figure 5.3 shows a plot of cycle number vs capacity of two samples. Both of them show a good cycle ability. LTO-N-1 shows a better stability of cycling which is also due to the introducing of new structure. The regular LTO has a capacity ramp at the first several cycle which may be considered as a bad performance. But the commercial batteries can avoid this since the charging-discharging process will be conducted several time before the battery get into use.

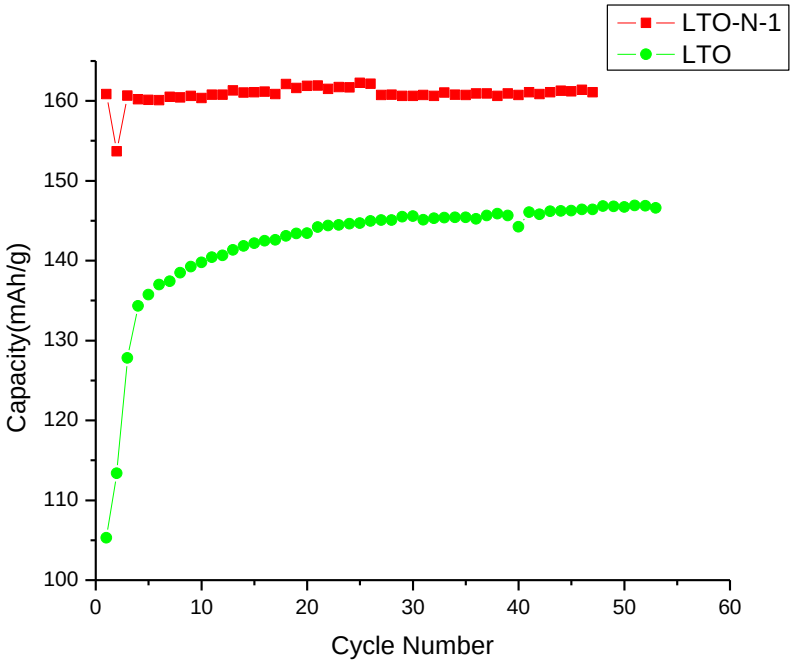

Figure 5.3 Relation between cycle number and capacity of LTO anode material

Chapter 6 Conclusion

In our research, the stability of $Li_4Ti_5O_{12}$ was successfully studied by XRD measurement and half-quantitate calculation based on XRD results. By introducing a new method (RTP) to synthesis/process $Li_4Ti_5O_{12}$, we were able to introduce a new $Li_4Ti_5O_{12}$-$Li_2Ti_3O_7$ nano composite.

The components were also studied by changing the annealing environment (annealing temperature, holding time, and atmosphere). This shows a final state of LTO using rapid thermo annealing as a synthesis/reprocessing method can be reached when annealing temperature is higher than 900 ℃ or the holding time ≥ 60 seconds at 880 ℃, with a composition of 25.4% $Li_2Ti_3O_7$ and 74.6% $Li_4Ti_5O_{12}$.

The structure was checked by further TEM study including HR-TEM. The results were highly agree with both XRD and half-quantitate calculation of volume percentage and mass percentage.

Also, the electrochemical properties of annealed LTO has been studied which shows a better capacity and cycle ability at the cost of a bigger difference of discharging and charging working potential.

Reference

[1] Ikeda, H., Saito, T. & Tamura, H. in Proc. Manganese Dioxide Symp.Vol. 1 (eds Kozawa, A. & Brodd, R. H.) (IC sample Office, Cleveland, OH, 1975).

[2] Steele, B. C. H. in Fast Ion Transport in Solids (ed. Van Gool, W.) 103–109 (North- Holland Amsterdam, 1973).

[3] Armand, M. B. in Fast Ion Transport in Solids (ed. Van Gool, W.) 665–673 (North Holland Amsterdam, 1973).

[4] Whittingham, M. S. Electrochemical energy storage and intercalation chemistry. *Science*. 192 (1976) 1226.

[5] Whittingham, M. S. Chalcogenide battery. US Patent 4009052.

[6] M. B. Armand, Materials for Advanced Batteries, Plenum Press, New York, 1990.

[7] Goodenough and Mizhuchima, US 4302518, 1980.

[8] Thackeray and Goodenough, US 4507371, 1983.

[9] Sony Company, EP391281, 1989.

[10] J.-M. Tarascon, M. Armand, *Nature*, 414 (2001) 359.

[11] C. Zu, H. Li, *Energy Environ. Sci*., 4 (2011) 2614.

[12] P.Poizot, S. Laruelle, S. Grugeon, L. Dupont and J. M. Tarascon, *Nature*, 407(2000) 496.

[13] H. Chen, M. Armand, G. Demailly, F.Dolhem, P. Poizot and J. M. Tarascon, *ChemSusChem* 1(2008) 348.

[14] Q. Wang, H. Li, L. Chen, X. Huang, D. Zhong and E. Wang, *J. Electrochem. Soc.* 150(2003) A1281.

[15] S.S. Zhang, *J. Power Sources* 161 (2006) 1385–1391.

[16] T. Ohzuku, A. Ueda, N. Yamamoto, *J. Electrochem. Soc.* 142 (1995) 1431–1435.

[17] C.Y. Ouyang, Z.Y. Zhong, M.S. Lei, *Electrochem. Commun*. 9 (2007) 1107–1112.

[18] K.-S. Park, A. Benayad, D.-J. Kang, S.-G. Doo, J. *Am. Chem. Soc.* 130 (2008) 14930–14931.

[19] T. Ohzuku, A. Ueda, N. Yamamoto, *J. Electrochem. Soc*. 142 (1995) 1431.

[20] D. Peramunage, K.M. Abraham, *J. Electrochem. Soc*. 145 (1998) 2615.

[21] G.X. Wang, D.H. Bradhurst, S.X. Dou, H.K. Liu, *J. Power Sources* 83 (1999) 156.

[22] P.P. Prosini, R. Mancini, L. Petrucci, V. Contini, P. Villano, *Solid State Ion*. 144 (2001) 185.

[23] K. Ariyoshi, S. Yamamoto, T. Ohzuku, *J. Power Sources* 119–121 (2003) 959.

[24] E.M. Sorensen, S.J. Barry, H.K. Jung, J.R. Rondinelli, J.T. Vaughey, K.R. Poeppelmeier, *Chem. Mater*. 18 (2006) 482.

[25] R.K.B. Gover, J.R. Tolchard, H. Tukamoto, T. Murai, J.T.S. Irvine, *J. Electrochem. Soc*. 146 (1999) 4348.

[26] M.E. Arroyo y de Dompablo, E. Morán, A. Várez, F. Gracía-Alvarado, *Mater. Res. Bull*. 32 (1997) 993.

[27] F. Chen, R.G. Li, M. Hou, L. Liu, R. Wang, Z.H. Deng, *Electrochim. Acta* 51 (2005) 61.

[28] J.B. Boyce, J.C. Mikkelsen Jr., *Solid State Commun*. 31 (1979) 741.

[29] R.K.B. Gover, J.R. Tolchard, H. Tukamoto, T. Murai, J.T.S. Irvine, *J. Electrochem. Soc*. 146 (1999) 4348.

[30] M.E. Arroyo y de Dompablo, E. Morán, A. Várez, F. Gracía-Alvarado, *Mater. Res. Bull*. 32 (1997) 993

[31] F. Chen, R.G. Li, M. Hou, L. Liu, R. Wang, Z.H. Deng, Electrochim. Acta 51 (2005) 61